

A parametrix for the surface Stokes equation

Tristan Goodwill¹, Jeremy Hoskins², Zydrunas Gimbutas³, and Bowei Wu⁴

Abstract: We introduce an integral equation formulation of the surface Stokes equations, constructed using two-dimensional Stokeslets. The resulting integral equations are Fredholm integral equations of the second kind and can be discretized to high order using standard tools. Since the resulting discrete linear systems are dense, we describe and analyze a *proxy shell method* to construct fast direct solvers for these systems. The properties of our integral equation, and the performance of the resulting numerical scheme, are illustrated with several representative numerical examples.

Keywords: Surface Stokes equation, parametrix methods, fast direct solver, proxy points, higher order surface approximation

AMS subject classifications 65N38, 65N80, 65R20, 65D05

1 Introduction

The flow of thin fluid films occurs in foams, emulsions, and biological applications [2, 8, 48, 49, 52, 53]. In most such problems, the flow is governed by the Stokes (or Navier-Stokes) equations posed on a manifold embedded in three dimensions. Recently, there has been growing interest in developing numerical methods for solving surface Stokes equations and other surface fluid flow problems. These methods are predominantly finite element methods (FEM) [5, 6, 12, 13, 16, 22, 26, 27, 33, 35, 42–45, 50–52], though there also exist closest point methods which use finite difference discretizations [60]. In the FEM approach, the problem is discretized in one of two ways: either the surface is discretized using a *surface finite element method* (SFEM) with a fitted mesh living on the surface (e.g. [13]); or, in the *trace finite element method* (TraceFEM), an unfitted mesh is constructed in the ambient space around the surface and surface fields are expressed as traces of functions defined on the unfitted mesh (e.g. [44]). Due to the difficulties associated with building high order surface meshes and conforming finite elements, implementations of these methods have generally been limited to at most third order [5], though a fourth order method was recently implemented [35]. Another contributing factor to the difficulty of this class of problems is the condition that the fluid flow on a static surface must be tangential. This tangency is usually enforced through a Lagrange multiplier or a penalty term [5, 16, 23, 26, 27, 33, 45, 51], resulting in larger or poorly-conditioned linear systems. Alternatively, there are several methods that build this tangency directly into the approximation space [12, 13, 35]. A different approach is to introduce a stream function formulation of the surface Stokes equations [6, 22, 42, 43, 50], which automatically enforces tangency and divergence-free conditions at the cost of increasing the order of the PDE. See [5, 42] for more detailed comparisons of these methods.

In this work, we take a different approach, reducing the surface Stokes equations to a system of integral equations, which we then discretize with a high order collocation scheme. Conceptually, we follow the general procedure of [17], which describes a method for scalar elliptic equations. In essence, the method amounts to constructing suitable *analytic* right-preconditioners for the equations. Analytic preconditioner (or parametrix) methods have previously been used to solve Stokes problems in Euclidean space, including variable viscosity problems [37] and the compressible Stokes equations [4]. More generally, there is a long history of applying related methods to other problems including the Lippmann–Schwinger equation for Helmholtz problems with variable wavenumber [10, 38], and variable coefficient Maxwell’s equations [32].

In the present paper, the velocity field is represented as an integral over the surface of the two-dimensional Stokeslet against an unknown density. Adding a term to account for the incom-

¹University of Chicago, Chicago, IL (tgoodwill@uchicago.edu)

²Department of Statistics and Committee on Computational and Applied Mathematics, University of Chicago, USA and NSF-Simons National Institute for Theory and Mathematics in Biology, Chicago, IL (jeremyhoskins@uchicago.edu)

³National Institute of Standards and Technology, Boulder, CO (zydrunas.gimbutas@nist.gov)

⁴University of Massachusetts Lowell, Lowell, MA (bowei.wu@uml.edu)

compressibility conditions and inserting this representation into the surface Stokes equations gives a Fredholm second kind integral equation that can be solved for the unknown density. This approach has several advantages. First, the tangential conditions are enforced directly by the integral equation. Second, the nonlocal nature of the integral equations remove many of the difficulties of mesh generation, enabling the construction of higher order discretizations. In particular, the meshes do not need to be conforming, nor even watertight. Finally, the Fredholm structure of the integral equations guarantees that the discretized equations will be well-conditioned, even when adaptive refinement is used to resolve small-scale features.

On the other hand, the resulting integral equations give rise to dense matrices when discretized. For large problems this can become prohibitively expensive both in terms of the memory requirements and overall computation time. This feature is common to all integral equation methods and has necessitated the construction of a number of fast algorithms. Many of these algorithms are based on off-diagonal rank structure of the system matrix. We prove that our integral equation has the same rank structure, which enables the use of fairly standard fast algorithms, as well as the construction of fast direct solvers based on the approaches of [29, 36, 41, 54]. We test our solvers on a variety of examples. This rank structure is of independent interest, since our analysis applies to a much broader class of equations, in particular to the equations developed for scalar surface PDEs in [17].

The remainder of the paper is organized as follows. In Section 2 we define the surface Stokes equations and briefly review the relevant surface differential operators. Following this, in Section 3 we describe the derivation of our integral equation formulation of the surface Stokes equation and establish several key analytic properties. In Section 4 we summarize the procedure we use to discretize our system of integral equations, and in Section 5 we present and analyze a method for accelerating the solution of our discretized system. Finally, in Section 6 we demonstrate the performance of our method with several numerical examples.

2 The surface Stokes equation

Before stating the surface Stokes equations, we first review the definitions of certain differential operators on smooth, bounded surfaces without boundary. There are a number of equivalent definitions of these operators, and we give the one most convenient for our purposes.

Definition 1. *Let Γ be a smooth and bounded surface. Let \mathbf{n} be the normal to Γ , defined as the gradient of a signed distance function. Let f , \mathbf{v} , and A be a function, vector field, and 3-matrix-valued function defined on Γ . Let f^e be a function defined in neighborhood of Γ that is equal to f on Γ . Let \mathbf{v}^e and A^e be defined similarly. We define the following quantities [50].*

1. The projection onto the tangent bundle is

$$\mathcal{P} := I - \mathbf{n}\mathbf{n}^T. \quad (2.1)$$

2. The surface gradient of f is

$$\nabla_\Gamma f = \mathcal{P}\nabla f^e. \quad (2.2)$$

3. The surface gradient of \mathbf{v} is

$$\nabla_\Gamma \mathbf{v} = \mathcal{P}(\nabla \mathbf{v}^e)\mathcal{P}. \quad (2.3)$$

4. The surface divergence of \mathbf{v} is

$$\nabla_\Gamma \cdot \mathbf{v} = \text{tr}(\nabla_\Gamma \mathbf{v}). \quad (2.4)$$

5. The divergence of A is

$$\nabla_\Gamma \cdot A = \begin{pmatrix} \nabla_\Gamma \cdot (e_1^T A) \\ \nabla_\Gamma \cdot (e_2^T A) \\ \nabla_\Gamma \cdot (e_3^T A) \end{pmatrix}. \quad (2.5)$$

It can be easily verified using the product rule that these definitions are independent of the choice of normal extension of f , \mathbf{v} , or A . Throughout this work, we shall choose the extension of \mathbf{n} to be constant along normal lines.

In this paper we consider the surface Stokes equations

$$\begin{cases} -\frac{1}{2}\mathcal{P}\nabla_\Gamma \cdot (\nabla_\Gamma \mathbf{u} + (\nabla_\Gamma \mathbf{u})^T) + \nabla_\Gamma p = \mathcal{P}\mathbf{f}, \\ \nabla_\Gamma \cdot \mathbf{u} = g, \\ \mathbf{u} \cdot \mathbf{n} = 0. \end{cases} \quad (2.6)$$

The quantity $E[\mathbf{u}] = -\frac{1}{2}(\nabla_\Gamma \mathbf{u} + (\nabla_\Gamma \mathbf{u})^T)$ in the above expression is frequently referred to as the *stress tensor*. Since g is the divergence of a vector field on a closed surface, it must be mean-zero. Typically we look for divergence-free \mathbf{u} (i.e. $g = 0$). We also fix the null space of constant pressures by requiring that the pressure is mean-zero.

3 Reduction to an integral equation

To derive an integral equation formulation for the surface Stokes equations (2.6), we introduce the 2D Stokeslet and its associated pressure

$$G(\mathbf{x}, \mathbf{y}) = \mathcal{P} \left(-\log r I + \frac{\mathbf{r}\mathbf{r}^T}{r^2} \right) \quad \text{and} \quad P_G(\mathbf{x}, \mathbf{y}) = \frac{\mathbf{r}^T}{r^2}, \quad (3.1)$$

where \mathbf{r} is treated as a column vector. We also introduce the kernel

$$K(\mathbf{x}, \mathbf{y}) = \frac{1}{2\pi} \nabla_\Gamma \log r = \mathcal{P} \frac{\mathbf{r}}{2\pi r^2}. \quad (3.2)$$

Using these kernels, we seek to represent the solution \mathbf{u} to equations (2.6) via the ansatz

$$\begin{aligned} \mathbf{u}(\mathbf{r}) &= \mathcal{G}[\boldsymbol{\sigma}](\mathbf{r}) + \mathcal{K}[\mu](\mathbf{r}) := \int_\Gamma G(\mathbf{r}, \mathbf{r}') \boldsymbol{\sigma}(\mathbf{r}') d(\mathbf{r}') + \int_\Gamma K(\mathbf{r}, \mathbf{r}') \mu(\mathbf{r}') d(\mathbf{r}') \\ \text{and } p(\mathbf{r}) &= \mathcal{P}_G[\boldsymbol{\sigma}](\mathbf{r}) + \mu(\mathbf{r}) := \int_\Gamma P_G(\mathbf{r}, \mathbf{r}') \boldsymbol{\sigma}(\mathbf{r}') d(\mathbf{r}') + \mu(\mathbf{r}), \end{aligned} \quad (3.3)$$

where $\boldsymbol{\sigma}$ is an unknown tangential vector field, μ is an unknown scalar function on Γ . We note that this representation automatically satisfies the tangency condition $\mathbf{u} \cdot \mathbf{n} = 0$ for any densities $\boldsymbol{\sigma}$ and μ . In order to find an equation for $(\boldsymbol{\sigma}, \mu)$ that ensures that (\mathbf{u}, p) satisfies (2.6), we require expressions for the derivatives of our ansatz, which are given in the following subsection.

3.1 Derivative identities

In this subsection we summarize several relevant derivative identities related to the kernels defined in (3.1) and (3.2). In general, the proofs follow from straightforward, if tedious, application of the formulas in Definition 1 and, for ease of exposition, are omitted.

Lemma 1. *Let $\mathbf{v} : \Gamma \rightarrow \mathbb{R}^3$ be twice continuously differentiable and let \mathbf{v}^e be its smooth extension to a neighborhood of Γ . Then*

$$\nabla_\Gamma \cdot \nabla_\Gamma \mathcal{P}\mathbf{v} = \mathcal{P}(\Delta - \partial_n^2)\mathbf{v} - 2S^T(\nabla\mathbf{v})^T \mathbf{n} - ((\Delta - \partial_n^2)\mathbf{n})\mathbf{n} \cdot \mathbf{v} - SS^T\mathbf{v} - 2H\mathcal{P}(\mathbf{n} \cdot \nabla)\mathbf{v},$$

where $(\nabla\mathbf{v})_{i,j} = \partial_j \mathbf{v}_i$, $S_{i,j} := \partial_j n_i$ is the shape operator (see [13]) and $H = \frac{1}{2}\partial_j n_j$ is the mean curvature. Moreover,

$$\begin{aligned} \nabla_\Gamma \cdot (\nabla_\Gamma \mathcal{P}\mathbf{v})^T &= \mathcal{P}\nabla(\nabla \cdot \mathcal{P}_f \mathbf{v}) - 2H\mathcal{P}(\nabla\mathbf{v})^T \mathbf{n} - S(\mathbf{n} \cdot \nabla)\mathbf{v} - \mathcal{P}\nabla(\nabla \cdot \mathcal{P}_f \mathbf{n})\mathbf{n} \cdot \mathbf{v} \\ &\quad - S^T S^T \mathbf{v} - S^T (\nabla\mathbf{v})^T \mathbf{n} \end{aligned}$$

where \mathcal{P}_f denotes the ‘frozen’ projection matrix, i.e. its derivatives are taken to be zero.

The following corollaries are an immediate consequence of the above lemma.

Corollary 0.1. *Let $\mathbf{v} = \frac{\mathbf{r}\mathbf{r}^T}{r^2}\mathbf{w}$ for some constant vector $\mathbf{w} \in \mathbb{R}^3$. Then*

$$\begin{aligned} \mathcal{P}\nabla_\Gamma \cdot \nabla_\Gamma \mathcal{P}\mathbf{v} &= \frac{2}{r^2}\mathcal{P}\mathbf{w} - \frac{4}{r^4}(\mathbf{r} \cdot \mathbf{w})\mathcal{P}\mathbf{r} + \frac{4}{r^4}(\mathbf{n} \cdot \mathbf{w})(\mathbf{r} \cdot \mathbf{n})\mathcal{P}\mathbf{r} - \frac{8}{r^6}(\mathbf{r} \cdot \mathbf{n})^2(\mathbf{r} \cdot \mathbf{w})\mathcal{P}\mathbf{r} \\ &\quad - 2S\frac{\mathbf{n} \cdot \mathbf{r}}{r^2}\mathcal{P}\mathbf{w} + \frac{4(\mathbf{n} \cdot \mathbf{r})(\mathbf{r} \cdot \mathbf{w})}{r^4}S\mathbf{r} - \mathcal{P}((\Delta - \partial_n^2)\mathbf{n})\frac{(\mathbf{n} \cdot \mathbf{r})(\mathbf{r} \cdot \mathbf{w})}{r^2} - \frac{\mathbf{r} \cdot \mathbf{w}}{r^2}S^2\mathbf{r} \\ &\quad - \frac{2(\mathbf{n} \cdot \mathbf{v})H}{r^2}\mathcal{P}\mathbf{r} + \frac{4(\mathbf{r} \cdot \mathbf{w})(\mathbf{r} \cdot \mathbf{n})H}{r^4}\mathcal{P}\mathbf{r} \end{aligned} \quad (3.4)$$

and

$$\begin{aligned} \nabla_\Gamma \cdot (\nabla_\Gamma \mathcal{P}\mathbf{v})^T &= -\frac{2(\mathbf{r} \cdot \mathbf{n})H}{r^2}\mathcal{P}\mathbf{w} + \frac{4(\mathbf{n} \cdot \mathbf{r})(\mathbf{r} \cdot \mathbf{w})H}{r^4}\mathcal{P}\mathbf{w} \\ &\quad + \frac{1}{r^2}\mathcal{P}\mathbf{w} - \frac{2(\mathbf{r} \cdot \mathbf{w})}{r^4}\mathcal{P}\mathbf{r} + \frac{2(\mathbf{n} \cdot \mathbf{r})(\mathbf{n} \cdot \mathbf{w})}{r^4}\mathcal{P}\mathbf{r} + \frac{2(\mathbf{r} \cdot \mathbf{n})^2}{r^4}\mathcal{P}\mathbf{w} - \frac{8(\mathbf{r} \cdot \mathbf{n})^2(\mathbf{r} \cdot \mathbf{w})}{r^6}\mathcal{P}\mathbf{r} \\ &\quad - \frac{\mathbf{n} \cdot \mathbf{w}}{r^2}S\mathbf{r} + \frac{2(\mathbf{r} \cdot \mathbf{n})(\mathbf{r} \cdot \mathbf{w})}{r^4}S\mathbf{r} - \frac{(\mathbf{n} \cdot \mathbf{r})(\mathbf{r} \cdot \mathbf{w})}{r^2}\mathcal{P}\nabla(\nabla \cdot \mathcal{P}_f\mathbf{n}) - \frac{\mathbf{r} \cdot \mathbf{w}}{r^2}S^2\mathbf{r} \\ &\quad - S\frac{\mathbf{n} \cdot \mathbf{r}}{r^2}\mathcal{P}\mathbf{w} + \frac{2(\mathbf{n} \cdot \mathbf{r})(\mathbf{r} \cdot \mathbf{w})}{r^4}S\mathbf{r}. \end{aligned} \quad (3.5)$$

Finally, we also have

$$\begin{aligned} \nabla_\Gamma \cdot (\nabla \mathcal{P} \log(r)\mathbf{w} + (\nabla_\Gamma \log(r)\mathcal{P}\mathbf{w})^T) &= \\ 4\pi\delta(r)\mathcal{P}\mathbf{w} + 2\frac{(\mathbf{n} \cdot \mathbf{r})^2}{r^4}\mathcal{P}\mathbf{w} - 3S\mathbf{r}\frac{\mathbf{w} \cdot \mathbf{n}}{r^2} - 2\log(r)(\mathbf{n} \cdot \mathbf{w})\mathcal{P}\Delta_\Gamma^{\text{comp}}\mathbf{n} - 2\log(r)S^2\mathbf{w} \\ - 2H\frac{\mathbf{n} \cdot \mathbf{r}}{r^2}\mathcal{P}\mathbf{w} + \frac{1}{r^2}\mathcal{P}\mathbf{w} - 2\frac{r^T\mathcal{P}\mathbf{w}}{r^4}\mathcal{P}\mathbf{r} - 2H\mathcal{P}\mathbf{r}\frac{\mathbf{w} \cdot \mathbf{n}}{r^2} - \frac{\mathbf{n} \cdot \mathbf{r}}{r^2}S\mathbf{w}, \end{aligned} \quad (3.6)$$

where $\Delta_\Gamma^{\text{comp}}$ denotes the componentwise Laplace-Beltrami operator.

The following lemma similarly follows straightforwardly from the formulas in Definition 1.

Lemma 2. *Let $\mathbf{v} = \frac{\mathbf{r}\mathbf{r}^T}{r^2}\mathbf{w}$ for some constant vector $\mathbf{w} \in \mathbb{R}^3$. Then*

$$\nabla_\Gamma \mathbf{v} = \frac{1}{r^2}\mathcal{P}\mathbf{w} - 2\frac{\mathcal{P}\mathbf{r}\mathbf{r}^T}{r^4}\mathbf{w}. \quad (3.7)$$

We summarize these results in the following theorem.

Theorem 1. *Let*

$$L[\mathbf{r}, \mathbf{w}] := \mathcal{P}\nabla_\Gamma \cdot E \left[-\log(r)\mathcal{P}\mathbf{w} + \mathcal{P}\frac{r\mathbf{r}^T}{r^2}\mathbf{w} \right] + \nabla_\Gamma \frac{r^T}{r^2}\mathbf{w}$$

where $\mathbf{w} \in \mathbb{R}^3$ is a constant vector. Then

$$\begin{aligned} L &= 2\pi\delta(r)\mathcal{P}\mathbf{w} - \frac{2}{r^4}(\mathbf{n} \cdot \mathbf{w})(\mathbf{r} \cdot \mathbf{n})\mathcal{P}\mathbf{r} + \frac{4}{r^6}(\mathbf{r} \cdot \mathbf{n})^2(\mathbf{r} \cdot \mathbf{w})\mathcal{P}\mathbf{r} + S\frac{\mathbf{n} \cdot \mathbf{r}}{r^2}\mathcal{P}\mathbf{w} - \frac{2(\mathbf{n} \cdot \mathbf{r})(\mathbf{r} \cdot \mathbf{w})}{r^4}S\mathbf{r} \\ &\quad + \frac{(\mathbf{n} \cdot \mathbf{r})^2}{r^4}\mathcal{P}\mathbf{w} - \frac{3}{2}S\mathbf{r}\frac{\mathbf{w} \cdot \mathbf{n}}{r^2} - \log(r)(\mathbf{n} \cdot \mathbf{w})\mathcal{P}\Delta_\Gamma^{\text{comp}}\mathbf{n} - \log(r)S^2\mathbf{w} - H\frac{\mathbf{n} \cdot \mathbf{r}}{r^2}\mathcal{P}\mathbf{w} \\ &\quad - H\mathcal{P}\mathbf{r}\frac{\mathbf{w} \cdot \mathbf{n}}{r^2} - \frac{\mathbf{n} \cdot \mathbf{r}}{2r^2}S\mathbf{w} + \frac{(\mathbf{r} \cdot \mathbf{n})H}{r^2}\mathcal{P}\mathbf{w} - \frac{2(\mathbf{n} \cdot \mathbf{r})(\mathbf{r} \cdot \mathbf{w})H}{r^4}\mathcal{P}\mathbf{w} \\ &\quad + \frac{1}{2}\mathcal{P}((\Delta - \partial_n^2)\mathbf{n})\frac{(\mathbf{n} \cdot \mathbf{r})(\mathbf{r} \cdot \mathbf{w})}{r^2} + \frac{1}{2}\frac{\mathbf{r} \cdot \mathbf{w}}{r^2}S^2\mathbf{r} + \frac{(\mathbf{n} \cdot \mathbf{w})H}{r^2}\mathcal{P}\mathbf{r} - \frac{2(\mathbf{r} \cdot \mathbf{w})(\mathbf{r} \cdot \mathbf{n})H}{r^4}\mathcal{P}\mathbf{r} \\ &\quad - \frac{(\mathbf{n} \cdot \mathbf{r})(\mathbf{n} \cdot \mathbf{w})}{r^4}\mathcal{P}\mathbf{r} - \frac{(\mathbf{r} \cdot \mathbf{n})^2}{r^4}\mathcal{P}\mathbf{w} + \frac{4(\mathbf{r} \cdot \mathbf{n})^2(\mathbf{r} \cdot \mathbf{w})}{r^6}\mathcal{P}\mathbf{r} + \frac{\mathbf{n} \cdot \mathbf{w}}{2r^2}S\mathbf{r} - \frac{(\mathbf{r} \cdot \mathbf{n})(\mathbf{r} \cdot \mathbf{w})}{r^4}S\mathbf{r} \\ &\quad + \frac{(\mathbf{n} \cdot \mathbf{r})(\mathbf{r} \cdot \mathbf{w})}{2r^2}\mathcal{P}\nabla(\nabla \cdot \mathcal{P}_f\mathbf{n}) + \frac{\mathbf{r} \cdot \mathbf{w}}{2r^2}S^2\mathbf{r} + S\frac{\mathbf{n} \cdot \mathbf{r}}{2r^2}\mathcal{P}\mathbf{w} - \frac{(\mathbf{n} \cdot \mathbf{r})(\mathbf{r} \cdot \mathbf{w})}{r^4}S\mathbf{r} + \frac{(\mathbf{n} \cdot \mathbf{r})(\mathbf{n} \cdot \mathbf{w})}{r^4}\mathcal{P}\mathbf{r}. \end{aligned}$$

For notational convenience, we define the following function.

Definition 2. With $L[\mathbf{r}, \mathbf{w}]$ defined as in the previous theorem, let

$$K_{G,1}(\mathbf{r}, \mathbf{r}')[\mathbf{w}] := L[\mathbf{r} - \mathbf{r}', \mathcal{P}(\mathbf{r}')\mathbf{w}] - 2\pi\delta(\mathbf{r} - \mathbf{r}')\mathcal{P}(\mathbf{r}')\mathbf{w}.$$

In particular, $K_{G,1}(\mathbf{r}, \mathbf{r}')$ is the matrix-valued function obtained by excluding the delta function from L , and projecting \mathbf{w} to its tangential components.

The following lemma gives an expression for G when it is substituted in for \mathbf{u} in the left-hand side of the second equation of (2.6).

Lemma 3. Let

$$\mathbf{v} = \left(-\log(r)I + \frac{\mathbf{r}\mathbf{r}^T}{r^2} \right) \mathbf{w}.$$

Then

$$\nabla_\Gamma \cdot \mathcal{P}\mathbf{v} = 2 \left[\frac{(\mathbf{n} \cdot \mathbf{r})^2(\mathbf{r} \cdot \mathbf{w})}{r^4} + H \log(r) (\mathbf{n} \cdot \mathbf{w}) - H \frac{(\mathbf{n} \cdot \mathbf{r})(\mathbf{r} \cdot \mathbf{w})}{r^2} \right]. \quad (3.8)$$

For notational convenience, we define the following function.

Definition 3. Let $k_{G,2}$ be the function defined by

$$k_{G,2}(\mathbf{r})[\mathbf{w}] := 2 \left[\frac{(\mathbf{n} \cdot \mathbf{r})^2(\mathbf{r} \cdot \mathbf{w})}{r^4} + H \log(r) (\mathbf{n} \cdot \mathbf{w}) - H \frac{(\mathbf{n} \cdot \mathbf{r})(\mathbf{r} \cdot \mathbf{w})}{r^2} \right] \quad (3.9)$$

where $\mathbf{w} \in \mathbb{R}^3$, and $K_{G,2}$ be defined by

$$K_{G,2}(\mathbf{r}, \mathbf{r}')[\mathbf{w}] := k_{G,2}(\mathbf{r} - \mathbf{r}')\mathcal{P}(\mathbf{r}')\mathbf{w}. \quad (3.10)$$

The following lemma gives the derivative of K when substituted into the first equation.

Lemma 4. Let $\mathbf{v} = \nabla_\Gamma \log r$. Then

$$\begin{aligned} \mathcal{P}\nabla_\Gamma \cdot (\nabla_\Gamma \mathbf{v} + (\nabla_\Gamma \mathbf{v})^T) &= 2\pi\mathcal{P}\nabla\delta(\mathbf{r}) \\ &- 8\frac{(\mathbf{n} \cdot \mathbf{r})^2}{r^6}\mathcal{P}\mathbf{r} + \frac{4(\mathbf{r} \cdot \mathbf{n})}{r^4}S\mathbf{r} - [(\Delta - \partial_n^2)\mathbf{n}]\frac{\mathbf{n} \cdot \mathbf{r}}{r^2} - \frac{1}{r^2}S^2\mathbf{r} + \frac{4H(\mathbf{n} \cdot \mathbf{r})}{r^4}\mathcal{P}\mathbf{r} \\ &+ \frac{4H(\mathbf{r} \cdot \mathbf{n})}{r^4}\mathcal{P}\mathbf{r} - \frac{8(\mathbf{n} \cdot \mathbf{r})^2}{r^6}\mathcal{P}\mathbf{r} + \frac{2(\mathbf{n} \cdot \mathbf{r})}{r^4}S\mathbf{r} - \mathcal{P}\nabla(\nabla \cdot \mathcal{P}_f\mathbf{n})\frac{(\mathbf{n} \cdot \mathbf{r})}{r^2} \\ &- \frac{1}{r^2}S^2\mathbf{r} + \frac{2(\mathbf{r} \cdot \mathbf{n})}{r^4}S\mathbf{r}. \end{aligned} \quad (3.11)$$

The previous lemma motivates the following definition.

Definition 4. Let $k_{K,1}$ be the vector-valued function defined by

$$\begin{aligned} 2\pi k_{K,1}(\mathbf{r}) &= -8\frac{(\mathbf{n} \cdot \mathbf{r})^2}{r^6}\mathcal{P}\mathbf{r} + \frac{4(\mathbf{r} \cdot \mathbf{n})}{r^4}S\mathbf{r} - [(\Delta - \partial_n^2)\mathbf{n}]\frac{\mathbf{n} \cdot \mathbf{r}}{r^2} - \frac{1}{r^2}S^2\mathbf{r} + \frac{4H(\mathbf{n} \cdot \mathbf{r})}{r^4}\mathcal{P}\mathbf{r} \\ &+ \frac{4H(\mathbf{r} \cdot \mathbf{n})}{r^4}\mathcal{P}\mathbf{r} - \frac{8(\mathbf{n} \cdot \mathbf{r})^2}{r^6}\mathcal{P}\mathbf{r} + \frac{2(\mathbf{n} \cdot \mathbf{r})}{r^4}S\mathbf{r} - \mathcal{P}\nabla(\nabla \cdot \mathcal{P}_f\mathbf{n})\frac{(\mathbf{n} \cdot \mathbf{r})}{r^2} \\ &- \frac{1}{r^2}S^2\mathbf{r} + \frac{2(\mathbf{r} \cdot \mathbf{n})}{r^4}S\mathbf{r}. \end{aligned} \quad (3.12)$$

and

$$K_{K,1}(\mathbf{r}, \mathbf{r}') := k_{K,1}(\mathbf{r} - \mathbf{r}'). \quad (3.13)$$

We conclude with the following lemma and corresponding definition.

Lemma 5. Let $\mathbf{v} = P \frac{\mathbf{r}}{2\pi r^2}$. Then

$$\nabla_\Gamma \cdot \mathbf{v} = \delta(\mathbf{r}) + \frac{2(\mathbf{n} \cdot \mathbf{r})^2}{2\pi r^4} - 2H \frac{\mathbf{n} \cdot \mathbf{r}}{2\pi r^2}. \quad (3.14)$$

Associated with the above identity, we have the following definition.

Definition 5. Let $k_{K,2}$ be the function defined by

$$k_{K,2}(\mathbf{r}) = \frac{2(\mathbf{n} \cdot \mathbf{r})^2}{2\pi r^4} - 2H \frac{\mathbf{n} \cdot \mathbf{r}}{2\pi r^2}. \quad (3.15)$$

and $K_{K,2}$ be defined by

$$K_{K,2}(\mathbf{r}, \mathbf{r}') = k_{K,2}(\mathbf{r} - \mathbf{r}'). \quad (3.16)$$

3.2 The integral equation and its properties

Collecting the identities given in the previous section, we see that if the ansatz (3.3) is substituted into the first and second equations of (2.6) then we obtain the following system of integral equations for the unknown densities σ and μ ,

$$2\pi\sigma + \mathcal{K}_{G,1}[\sigma] + \mathcal{K}_{K,1}[\mu] = \mathcal{P}\mathbf{f} \quad (3.17)$$

$$\mu + \mathcal{K}_{G,2}[\sigma] + \mathcal{K}_{K,2}[\mu] = g, \quad (3.18)$$

where $\mathcal{K}_{G,1}, \mathcal{K}_{G,2}, \mathcal{K}_{K,1}$, and $\mathcal{K}_{K,2}$ are the integral operators with kernels $K_{G,1}, K_{G,2}, K_{K,1}$, and $K_{K,2}$ given in Definitions 2, 3, 4, and 5, respectively (defined analogously to (3.3)).

Remark 1. For notational convenience, and ease of exposition, we have written the above equation for $\sigma : \Gamma \rightarrow \mathbb{R}^3$, rather than explicitly parameterizing it as a tangential vector field. The fact that a σ obtained from solving these equations is indeed tangential can be deduced by taking the inner product of (3.17) with \mathbf{n} and observing that $\mathbf{n} \cdot \mathcal{K}_{G,1} = 0 = \mathbf{n} \cdot \mathcal{K}_{K,1}$.

The following theorem establishes important properties of the operators appearing in the integral equation system (3.17,3.18).

Theorem 2. Let $\mathcal{K}_{G,1}, \mathcal{K}_{G,2}, \mathcal{K}_{K,1}$, and $\mathcal{K}_{K,2}$ be the integral operators with kernels $K_{G,1}, K_{G,2}, K_{K,1}$, and $K_{K,2}$ given in Definitions 2, 3, 4, and 5, respectively. If Γ is a smooth and compact manifold without boundary then for any $p \in \mathbb{R}_{\geq 0}$ and any $\epsilon \in (0, 1]$,

1. $\mathcal{K}_{G,1} : H^p(\Gamma; \mathbb{R}^3) \rightarrow H^{p+2-\epsilon}(\Gamma; \mathbb{R}^3)$
2. $\mathcal{K}_{G,2} : H^p(\Gamma; \mathbb{R}^3) \rightarrow H^{p+2-\epsilon}(\Gamma; \mathbb{R})$
3. $\mathcal{K}_{K,1} : H^p(\Gamma; \mathbb{R}) \rightarrow H^{p+1-\epsilon}(\Gamma; \mathbb{R}^3)$, and
4. $\mathcal{K}_{K,2} : H^p(\Gamma; \mathbb{R}) \rightarrow H^{p+2-\epsilon}(\Gamma; \mathbb{R})$,

where H^p denotes the standard Sobolev space on Γ . Moreover, for any $p \geq 0$, as operators from $H^p \rightarrow H^p$, all of the above operators are compact.

Proof. We prove this result by identifying the singularities of the kernels when $\mathbf{r} \approx \mathbf{r}'$. We begin by identifying, and Taylor expanding, a few prototypical singular terms. For a smooth surface Γ , if $\mathbf{r} : \mathbb{R}^2 \rightarrow \Gamma$ is a local coordinate system then

$$\begin{aligned} \mathbf{r}(u, v) - \mathbf{r}(u', v') &= \mathbf{r}_u(u', v')(u - u') + \mathbf{r}_v(u', v')(v - v') + \frac{1}{2}\mathbf{r}_{uu}(u', v')(u - u')^2 + \\ &+ \mathbf{r}_{uv}(u', v')(u - u')(v - v') + \frac{1}{2}\mathbf{r}_{vv}(u', v')(v - v')^2 + O((u - u')^3 + (v - v')^3), \end{aligned}$$

where subscripts denote partial derivatives. It follows immediately that

$$(\mathbf{r}(u, v) - \mathbf{r}'(u', v')) \cdot \mathbf{n}(u', v') = \mathbb{I}(\mathbf{u}' - \mathbf{v}') + O((u - u')^3 + (v - v')^3), \quad (3.19)$$

where $\mathbf{u} = (u, v)$, $\mathbf{u}' = (u', v')$, and \mathbb{I} denotes the second fundamental form at (u', v') . Similarly,

$$\|\mathbf{r}(u, v) - \mathbf{r}'(u', v')\|^2 = \mathbb{I}(\mathbf{u} - \mathbf{u}') + O((u - u')^3 + (v - v')^3),$$

where \mathbb{I} denotes the first fundamental form. In particular, it follows immediately (see [31] for example) that

$$F(u, v; u', v') := \frac{(\mathbf{r}(u, v) - \mathbf{r}'(u', v')) \cdot \mathbf{n}(u', v')}{\|\mathbf{r}(u, v) - \mathbf{r}'(u', v')\|^2} = \kappa_{u', v'}(\mathbf{u} - \mathbf{u}') + O(\|\mathbf{u} - \mathbf{u}'\|) \quad (3.20)$$

where $\kappa_{u', v'}$ denotes the normal curvature of Γ at the point $\mathbf{r}'(u', v')$. We further note that the $O(\|\mathbf{u} - \mathbf{u}'\|)$ remainder is differentiable in u and v except at (u', v') , and the derivatives are bounded in the vicinity of (u', v') . It is similarly easy to show that $\nabla_{(u, v)}F$ and $\nabla_{(u', v')}F$ are both of the form $\frac{G_F(u, v; u', v')}{\|\mathbf{u} - \mathbf{u}'\|}$ where G_F is bounded, and smooth away from the diagonal. If we set $F^*(u, v; u', v') = F(u', v'; v, u)$ then similar arguments show that F^* satisfies all of the same estimates as F .

Next, we consider

$$R(u, v; u', v') := \frac{1}{\|\mathbf{r}(u, v) - \mathbf{r}'(u', v')\|} \mathcal{P}(u', v') \mathbf{n}(u, v),$$

where $\mathcal{P}(u', v')$ is the 3×3 projection matrix onto the tangent plane at (u', v') . Performing a Taylor expansion on \mathbf{n} , we find

$$\begin{aligned} \mathbf{n}(u, v) &= \mathbf{n}(u', v') + S\mathbf{r}_u(u', v')(u - u') + S\mathbf{r}_v(u', v')(v - v') + O(\|\mathbf{u} - \mathbf{u}'\|^2), \\ &= \mathbf{n}(u', v') + S(\mathbf{r}(u, v) - \mathbf{r}'(u', v')) + O(\|\mathbf{u} - \mathbf{u}'\|^2), \end{aligned}$$

where S is the shape operator of Γ at $\mathbf{r}'(u', v')$. Thus,

$$R(u, v; u', v') = S \frac{\mathbf{r}(u, v) - \mathbf{r}'(u', v')}{\|\mathbf{r}(u, v) - \mathbf{r}'(u', v')\|} + O(\|\mathbf{r}(u, v) - \mathbf{r}'(u', v')\|).$$

As for F , we note that the remainder is differentiable in u and v except at (u', v') with bounded derivatives, at least in the vicinity of (u', v') . It is also clear that $\nabla_{(u, v)}R$ and $\nabla_{(u', v')}R$ are both of the form $\frac{G_R(u, v; u', v')}{\|\mathbf{u} - \mathbf{u}'\|}$ where G_R is bounded, and smooth away from the diagonal. If we set $R^*(u, v; u', v') = R(u', v'; v, u)$ then similar arguments show that R^* satisfies all of the same estimates as R .

Finally, we observe that if

$$T(u, v; u', v') := \frac{(\mathbf{r}(u, v) - \mathbf{r}'(u', v'))}{\|\mathbf{r}(u, v) - \mathbf{r}'(u', v')\|},$$

then $\nabla_{(u, v)}T$ and $\nabla_{(u', v')}T$ are both of the form $\frac{G_T(u, v; u', v')}{\|\mathbf{u} - \mathbf{u}'\|}$ where G_H is bounded, and smooth away from the diagonal.

Looking at Definitions 2, 3, 5 we can see that all of the terms in $K_{G,1}$, $K_{G,2}$, and $K_{K,2}$ are of the form $\varphi(\mathbf{u}, \mathbf{u}', F, F^*, R, R^*, T) + \log(r)M$, where $\varphi : \Gamma \times \Gamma \times \mathbb{R}^5 \rightarrow \mathbb{R}^{j \times k}$, $j, k \in \{1, 2, 3\}$, and $M \in H^2(\Gamma; \mathbb{R}^{j \times k})$ is a (possibly matrix-valued) function on Γ . The derivatives of these kernels have at most a $1/\|\mathbf{u} - \mathbf{u}'\|$ singularity near the diagonal, and so standard results on weakly-singular integral operators (e.g. Theorem 4.1 in [46]) give that the derivatives of the integral operator \mathcal{K} with kernel map $H^p(\Gamma; \mathbb{R}^j) \rightarrow H^{p+1-\epsilon}(\Gamma; \mathbb{R}^k)$ for any non-negative p . Thus \mathcal{K} itself maps $H^p(\Gamma; \mathbb{R}^j) \rightarrow H^{p+2-\epsilon}(\Gamma; \mathbb{R}^k)$ for any $\epsilon \in (0, 1]$, and any $p \in \mathbb{R}_{\geq 0}$ and we have proved the desired mapping properties of $\mathcal{K}_{G,1}$, $\mathcal{K}_{G,2}$, and $\mathcal{K}_{K,2}$.

The last kernel, $K_{K,1}$, contains terms of the form

$$\varphi(\mathbf{u}, \mathbf{u}', F, F^*, R, R^*, T) \frac{\mathbf{r}}{r^2},$$

in addition to terms of the above form. It follows that $\mathcal{K}_{K,1} : H^p(\Gamma; \mathbb{R}) \rightarrow H^{p+1-\epsilon}(\Gamma; \mathbb{R}^3)$, from similar reasoning as above. The compactness of the integral operators then follows from their mapping properties and the Sobolev embedding theorem. \square

The following corollary is an immediate but important consequence of the previous theorem.

Corollary 2.1. *The system of integral equations (3.17,3.18) are Fredholm-second kind. In particular, existence and uniqueness are equivalent, and the space of solutions to the homogeneous problem (with $\mathcal{P}\mathbf{f} = g = 0$) is finite dimensional.*

A standard bootstrapping argument establishes improved regularity of $\boldsymbol{\sigma}$ and μ if $\mathcal{P}\mathbf{f}$ and g are $C^k(\Gamma)$. The proof follows immediately from the mapping properties of $\mathcal{K}_{G,1}, \dots, \mathcal{K}_{K,2}$.

Corollary 2.2. *Let $\boldsymbol{\sigma}$ and μ be solutions to (3.17,3.18) with right-hand sides $\mathcal{P}\mathbf{f} \in C^k(\Gamma, \mathbb{R}^3)$ and $g \in C^{k+1}(\Gamma, \mathbb{R})$ for $k > 1$. Then $\boldsymbol{\sigma} \in C^k(\Gamma, \mathbb{R}^3)$ and $\mu \in C^k(\Gamma, \mathbb{R})$.*

As noted above, solvability of (2.6) requires g to be mean zero. We also note that the pressure p is only defined up to a constant, and so we are free to impose the additional constraint that μ be mean-zero (see [17, 47]). It is easily seen that the addition of this condition leads to the modified equations:

$$2\pi\boldsymbol{\sigma} + \mathcal{K}_{G,1}[\boldsymbol{\sigma}] + \mathcal{K}_{K,1}[\mu] = \mathcal{P}\mathbf{f} \quad (3.21)$$

$$\mu + \frac{1}{|\Gamma|} \int_{\Gamma} \mu + \mathcal{K}_{G,2}[\boldsymbol{\sigma}] + \mathcal{K}_{K,2}[\mu] = g, \quad (3.22)$$

where $|\Gamma|$ is the area of Γ . In particular, the divergence theorem applied to (3.22) recovers the condition $\int \mu = 0$.

Remark 2. *It is well-known that if Γ has non-trivial Killing vector fields then the PDE (2.6) will have non-trivial homogeneous solutions. The corresponding nullspace of the left-hand side of the system (3.21,3.22) can be determined and dealt with using standard methods, see for example [47].*

Remark 3. *In many papers on computational methods for the surface Stokes equations, a linear term proportional to \mathbf{u} is added to the first equation of (2.6) to avoid the necessity of dealing with subtle questions of solvability associated with the Killing fields. The addition of this term is easily treated within our integral equation framework and amounts to a compact perturbation of the system (3.21,3.22). The resulting system is therefore also Fredholm-second kind.*

For notational convenience we set $\boldsymbol{\rho} = (\boldsymbol{\sigma}, \mu)^T$ and let \mathcal{K}_T be the integral operator with matrix-valued kernel

$$K_T(\mathbf{r}, \mathbf{r}') = \begin{pmatrix} \frac{1}{2\pi} K_{G,1} & \frac{1}{2\pi} K_{K,1} \\ K_{G,2}(\mathbf{r}, \mathbf{r}') & K_{K,2}(\mathbf{r}, \mathbf{r}') + \frac{1}{|\Gamma|} \end{pmatrix}.$$

Setting $\mathbf{h} = (\frac{1}{2\pi}\mathcal{P}\mathbf{f}, g)^T$, our integral equations (3.21,3.22) can be re-written as

$$\boldsymbol{\rho} + \mathcal{K}_T[\boldsymbol{\rho}] = \mathbf{h}. \quad (3.23)$$

4 Discretization and Quadrature

In this section we describe a collocation approach for discretizing the system of integral equations (3.21,3.22). Though much of it is standard, and indeed our implementation mostly relies on standard tools as implemented in the package *fmm3dbie* [3], we sketch the details here in the interest of making the description as self-contained as possible.

4.1 Discretization of the system

Let T_0 denote the standard right-triangle $T_0 = \{(x, y) \in \mathbb{R}_{>0}^2 \mid x + y < 1\}$. We assume that the surface Γ is given as a set of smooth maps $\psi_i : T_0 \rightarrow \Gamma \subset \mathbb{R}^3$, $i = 1, \dots, I$ such that the sets $\Gamma_i := \psi_i(T_0)$, $i = 1, \dots, I$ are mutually disjoint and $\cup_{i=1}^I \psi_i(T_0) = \Gamma$. We also assume that the determinants of the metric tensors g_i of the maps ψ_i are bounded uniformly away from zero on the closure of T_0 .

We can then rewrite the integral equation (3.23) as

$$\boldsymbol{\rho}(\mathbf{r}) + \sum_{i=1}^I \int_{T_0} K_T(\mathbf{r}, \psi_i(u, v)) \boldsymbol{\rho}(\psi_i(u, v)) \sqrt{\det g_i(u, v)} da(u, v) = \mathbf{h}(\mathbf{r}). \quad (4.1)$$

We discretize this system using a collocation method. Suppose for the k th patch we fix a basis $\varphi_j^k : T_0 \rightarrow \mathbb{R}^4$, $j = 1, \dots, M$, and construct a corresponding M point discretization of T_0 with nodes (u_j^k, v_j^k) , $j = 1, \dots, M$ which gives stable interpolation of the basis functions φ_j^k . In particular, we require the matrix U^k with i, j th entry $U_{i,j}^k = \varphi_j^k(x_i^k)$, $1 \leq i, j \leq M$ to be well-conditioned. We then proceed by enforcing consistency only at these discretization nodes. In particular, if we set $\boldsymbol{\rho}_i(u, v) = \boldsymbol{\rho}(\psi_i(u, v))$ and $\mathbf{h}_i(u, v) = \mathbf{h}(\psi_i(u, v))$ then we require

$$\boldsymbol{\rho}_k(u_j^k, v_j^k) + \sum_{i=1}^I \int_{T_0} K_T(\psi_k(u_j^k, v_j^k), \psi_i(u, v)) \boldsymbol{\rho}_i(u, v) \sqrt{\det g_i(u, v)} da(u, v) = \mathbf{h}_k(u_j^k, v_j^k). \quad (4.2)$$

To continue, we need a quadrature rule for accurately approximating the integrals on the left-hand side of (4.2). Conceptually, if $\boldsymbol{\rho}_i$ is approximately in the span of the basis elements φ_i^k , $i = 1, \dots, M$, then

$$\boldsymbol{\rho}_i(u, v) \approx \sum_{j=1}^M \varphi_j^k(u, v) (U^k)_{j,k}^{-1} \boldsymbol{\rho}_i(u_k^i, v_k^i).$$

In particular, if we define the integrals

$$A_{j,\ell}^{k,i} := \sum_{n=1}^M \left[\int_{T_0} K_T(\psi_k(u_j^k, v_j^k), \psi_i(u, v)) \varphi_\ell^n(u, v) \sqrt{\det g_i(u, v)} da(u, v) \right] (U^k)_{n,\ell}^{-1} \quad (4.3)$$

then

$$\boldsymbol{\rho}_k(u_j^k, v_j^k) + \sum_{i=1}^I \sum_{\ell=1}^M A_{j,\ell}^{k,i} \boldsymbol{\rho}_i(u_\ell^i, v_\ell^i) \approx \mathbf{h}_k(u_j^k, v_j^k).$$

Letting $\hat{\boldsymbol{\rho}}_{j,k}$ denote our unknowns, our discrete system is given by

$$\hat{\boldsymbol{\rho}}_{j,k} + \sum_{i=1}^I \sum_{\ell=1}^M A_{j,\ell}^{k,i} \hat{\boldsymbol{\rho}}_{\ell,i} \approx \mathbf{h}_k(u_j^k, v_j^k). \quad (4.4)$$

In our implementation we choose our basis on T_0 to be the Koornwinder polynomials of degree at most q , which form an orthogonal basis of the monomials $u^j v^k$, $j, k \geq 0$, $j + k \leq q$. As discretization nodes, we choose the corresponding Vioreanu-Rokhlin nodes [57], see Figure 1. With this choice, $M = (q + 1)(q + 2)/2$.

Since we choose the same nodes on each patch, all of the interpolation matrices U_k are the same. We denote this matrix by U . The Vioreanu-Rokhlin nodes are constructed so that the resulting matrix U is well-conditioned. Moreover, associated with the points (u_j, v_j) are corresponding quadrature weights w_j such that the quadrature scheme with nodes (u_j, v_j) and weights w_j integrate all Koornwinder polynomials of degree at most q are integrated exactly.

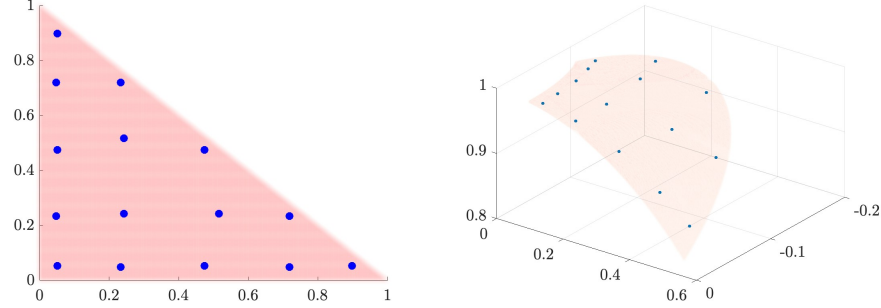


Figure 1: An illustration of the local discretization. Left: the Vioreanu-Rokhlin nodes of order 4 on the standard triangle T_0 . The nodes are shown in blue and T_0 is shaded red. Right: the image of the Vioreanu-Rokhlin nodes (blue) on a patch $\Gamma_i \subset \mathbb{R}^3$ (red).

4.2 Quadrature for weakly-singular integral operators

So far we have not addressed how the integrals $A_{j,\ell}^{k,i}$ in (4.3) are computed numerically. Here we give a brief description of our approach. We refer the interested reader to [20] for a more complete description of methods of this type. For a fixed ‘target’ patch number k we split the ‘source’ patches $i = 1, \dots, I$ into three categories: self (i.e. $i = k$), near (i.e. $i \neq k$ but $\text{dist}(\Gamma_k, \Gamma_i) < \alpha \min\{\text{diam}\Gamma_k, \text{diam}\Gamma_i\}$), and far (all patches which are not self or near). Here the constant α controls a trade-off between speed and accuracy. We again refer the reader to [20] for a detailed description of the choice of this parameter. In our numerical experiments we use the default settings of *fmm3dbie* [3, 7, 58].

4.2.1 Far quadrature

When the source patch Γ_i is sufficiently separated from the target patch Γ_k , the kernel $K_T(\psi_k(u_j^k, v_j^k), \psi_i(u, v))$ is in $C^\infty(\overline{T_0})$, viewed as a function of (u, v) . Similarly, so is the square root of the determinant of the metric tensor $\sqrt{\det g_i(u, v)}$. Thus, we can use the *native quadrature rule*, i.e.

$$A_{j,\ell}^{k,i} \approx \sum_{n=1}^M \sum_{m=1}^M \left[K_T(\psi_k(u_j^k, v_j^k), \psi_i(u_m^i, v_m^i)) \varphi_\ell^n(u_m^i, v_m^i) \sqrt{\det g_i(u_m^i, v_m^i)} w_m \right] (U^k)_{n,\ell}^{-1}, \quad (4.5)$$

$$\approx \sum_{m=1}^M \left[K_T(\psi_k(u_j^k, v_j^k), \psi_i(u_m^i, v_m^i)) \sqrt{\det g_i(u_m^i, v_m^i)} w_m \right] \quad (4.6)$$

where in going from the first line to the second we use the definition of U^k . In the following, we set $\omega_m^i := \sqrt{\det g_i(u_m^i, v_m^i)} w_m$.

Remark 4. *Depending on the order q of the discretization, it is sometimes convenient to oversample, i.e. use a higher-order Vioreanu-Rokhlin quadrature for the integrals. Though this yields more accurate computation of the desired integrals, the resulting formulas are more involved. In particular, in most applications it is too stringent to assume that one has an analytic form for the surface available at the time when quadratures are being constructed. Instead, the surface and its salient properties (normal derivatives, tangent vectors, curvature, shape operators, etc.) are also represented as Koornwinder polynomial expansions, interpolated from Vioreanu-Rokhlin nodes. See Figure 1 for an illustration. We once again refer the reader to [20] for a detailed discussion of this procedure and the corresponding desiderata.*

4.2.2 Near quadrature

When the source patch Γ_i is close to the target patch Γ_k , the kernel K_T is nearly-singular. It follows that it may have extremely slow decay in the coefficients of its expansion in the basis of Koornwinder

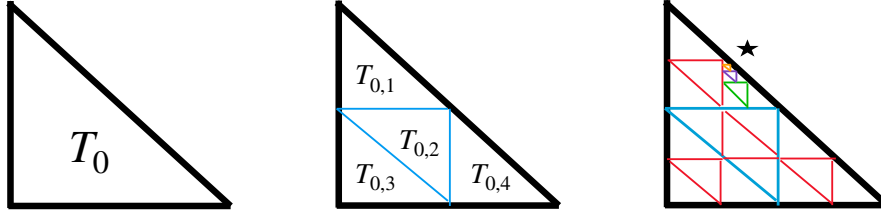


Figure 2: An illustration of the adaptive integration strategy used in the near-field integral computation. Left: the standard triangle T_0 . Middle: the first level of refinement. Right: a cartoon of the refinement used for a source located at the point indicated by a star.

polynomials. Thus, using either the native quadrature rule or the oversampling procedure in Remark 4 would be either inaccurate or impractical. Instead, we use adaptive integration. In practice, it is typically impractical to assume that we have access to an easily queried analytic parameterization of the surface F at this point in the calculation. Instead we replace the maps ψ_i by approximations $\hat{\psi}_i$ given by Koornwinder polynomial expansions. In particular, we store the values of ψ_i , $\partial_u \psi_i$, $\partial_v \psi_i$, and the first and second fundamental forms at the Vioreanu-Rokhlin nodes (u_j, v_j) . If the derivatives of ψ_i are not given analytically then approximations can be computed via spectral differentiation. Given these approximate maps we are then free to interpolate the relevant quantities to any point in T_0 .

Our adaptive integration proceeds as follows. First, we evaluate the matrix-entry integrals (4.3) via the standard native quadrature rule to obtain an approximation \hat{A}_0 (for ease of exposition we suppress the dependence on k, i, j and ℓ). We then cut T_0 into four triangles, $T_{0,1}, T_{0,2}, T_{0,3}$ and $T_{0,4}$, as in Figure 2. Next, we use rescaled Vioreanu-Rokhlin nodes and quadrature on each of these subtriangles, which we denote by $\hat{A}_{0,1}, \hat{A}_{0,2}, \hat{A}_{0,3}$, and $\hat{A}_{0,4}$, respectively. If $|\hat{A}_0 - \hat{A}_{0,1} - \hat{A}_{0,2} - \hat{A}_{0,3} - \hat{A}_{0,4}| < \epsilon$, where ϵ is a user-prescribed tolerance, then we use $\hat{A}_{0,1} + \dots + \hat{A}_{0,4}$ as our approximation. If the difference is above the tolerance then we subdivide $T_{0,1}, \dots, T_{0,4}$ each into four new triangles, giving T_{0,i_1,i_2} , $1 \leq i_1, i_2 \leq 4$, and construct corresponding Vioreanu-Rokhlin nodes and weights on each of these subtriangles to compute \hat{A}_{0,i_1,i_2} , $1 \leq i_1, i_2 \leq 4$. For each i_1 we compare \hat{A}_{0,i_1} with $\sum_{i_2=1}^4 \hat{A}_{0,i_1,i_2}$. If the difference is below the tolerance then we do not subdivide the triangles \hat{A}_{0,i_1,i_2} further. If not, then we once again cut each of the triangles into 4. We then proceed recursively, stopping when the sum of the approximate integrals over all the ‘leaf’ triangles (those without any children) are within the tolerance of their parent’s integrals. We then set our approximate integrals of A to be the sum computed using the quadrature rules on all of the leaf triangles.

Remark 5. *In practice it is better to use Xiao-Gimbutas [58] quadrature nodes to perform the integration in this setting. The order q Xiao-Gimbutas quadrature rule is designed to integrate more than the first $(q+1)(q+2)/2$ Koornwinder polynomials, and hence is more efficient than the same order Vioreanu-Rokhlin quadrature.*

Remark 6. *Other refinement strategies are possible. One common strategy is to refine each triangle until either all its subtriangles are separated from the target by a constant factor times their diameter or the triangles are sufficiently small that their contribution to the integral is less than the desired tolerance.*

4.2.3 Self quadrature

When the source patch and target patch coincide, the integrands will, in general, have slow or no decay in the coefficients of their Koornwinder polynomial expansion, and may have singularities in their derivatives as $(u, v) \rightarrow (u_j^k, v_j^k)$. In principle, the adaptive integration approach described in the previous subsection may still be used to approximate the integrals. In practice, this can become prohibitively slow, as many levels are required to resolve the singular behavior of the integrand. Instead, a standard approach is to use *generalized Gaussian quadratures* [7].

The first step is to apply an affine transformation $(u, v) \mapsto (\tilde{u}, \tilde{v})$ to T_0 with $(u_j^k, v_j^k) \mapsto (0, 0)$, which makes the first fundamental form of Γ_k the identity at $\psi_k(u_j^k, v_j^k) = \tilde{\psi}_k(0, 0)$, with respect to this new coordinate system. The triangle is then split into three subtriangles, each with a vertex at $(0, 0)$. On each of these triangles integrals are performed using appropriate quadratures, constructed via the approach in [7], which accurately integrate singularities of the form:

$$\frac{p_1(\tilde{u}, \tilde{v})}{\sqrt{\tilde{u}^2 + \tilde{v}^2}} + p_2(\tilde{u}, \tilde{v}) \log(\tilde{u}^2 + \tilde{v}^2) + p_3(\tilde{u}, \tilde{v})T(\cos \varphi, \sin \varphi) + p_4(\tilde{u}, \tilde{v})$$

for arbitrary polynomials p_1, p_2 , and p_3 of degree at most p (depending on the particular quadrature rule employed) and T is a polynomial in $(\cos \varphi, \sin \varphi) := (\tilde{u}, \tilde{v})/\sqrt{\tilde{u}^2 + \tilde{v}^2}$, to within a prefixed tolerance (typically machine precision or better).

5 Acceleration of the computation

The Faustian bargain we make when recasting the PDE system (2.6) as a system of integral equations is that we obtain a well-conditioned Fredholm second-kind system, but lose the sparsity that comes with discretizing local operators directly. Indeed, this is the *raison d'être* for a number of fast algorithms [20, 25, 30, 38, 39]. The majority of these algorithms are based on low rank factorizations of blocks of the discretized system matrix. In this section, we illustrate a simple algorithm reminiscent of the method presented in Chapter 13 of [38] for solving (4.4) that leverages these factorizations. More efficient solvers can be constructed by building hierarchical low rank factorizations (Chapter 14 of [38]) and in our numerical examples below we use the method described in [54], adapted to handle this vector-valued problem.

Typically, for standard fast algorithms such as *inter alia* the *fast multipole method* [21, 24, 55] and *fast direct solvers* [11, 19, 40, 41, 54], the method relies on the kernels satisfying a Green's identity. Though there are algorithms that only leverage smoothness of the function (for example [14, 28]), the overall computational cost can be significantly larger relative to the classical methods, depending on the form of the kernels and their associated rank structure. Our kernels fall between these two categories. While they do not satisfy Green's identities in three dimensions, they are built out of two dimensional fundamental solutions of PDEs and their derivatives. In this section, we show how to use this fact to analyze the rank structure of our discretized operators. The approach extends naturally to a much broader class of problems.

As motivation, we briefly sketch a simple compression-based algorithm which exploits a certain low rank structure of the system matrix A for solving systems like (4.4). We partition the surface Γ into n boxes, assuming each box has approximately equal number of discretization nodes, and let A_{ij} denote the sub-block of A corresponding to interactions between points in box j with points in box i . If we let ρ_i and h_i denote the degrees of freedom and data in box i respectively, then (4.4) is equivalent to the block-system

$$\begin{pmatrix} A_{11} & \cdots & A_{1n} \\ \vdots & & \vdots \\ A_{n1} & \cdots & A_{nn} \end{pmatrix} \begin{pmatrix} \rho_1 \\ \vdots \\ \rho_n \end{pmatrix} = \begin{pmatrix} h_1 \\ \vdots \\ h_n \end{pmatrix}. \quad (5.1)$$

In the next section we will show that for each box B_i there exist rectangular matrices $X_i \in \mathbb{R}^{N_i \times N_{s,i}}$ and $E_i \in \mathbb{R}^{N_{s,i} \times N_i}$, $N_{s,i} < N_i$ such that each sub-block A_{ij} with $i \neq j$ admits the approximate low-rank factorization

$$A_{ij} \approx E_i \hat{A}_{ij} X_j, \quad (5.2)$$

where \hat{A}_{ij} is a sub-matrix of A_{ij} . Let $\tau = \max_i N_{s,i}/N_i$. Assuming for now that we have such an approximate factorization, if we substitute it into our system and multiply each row by A_{ii}^{-1} ,

then (5.1) becomes

$$\begin{pmatrix} I & A_{11}^{-1}E_1\hat{A}_{12}X_2 & \cdots & A_{11}^{-1}E_1\hat{A}_{1n}X_n \\ \vdots & & & \vdots \\ A_{nn}^{-1}E_n\hat{A}_{n1}X_1 & \cdots & A_{nn}^{-1}E_n\hat{A}_{n(n-1)}X_{n-1} & I \end{pmatrix} \begin{pmatrix} \rho_1 \\ \vdots \\ \rho_n \end{pmatrix} = \begin{pmatrix} A_{11}^{-1}h_1 \\ \vdots \\ A_{nn}^{-1}h_n \end{pmatrix}. \quad (5.3)$$

To continue, we introduce the *skeleton variables* $\hat{\rho}_i = X_i\rho_i$ for all i . If we solve for each $\hat{\rho}_i$, then we can use the above equations to easily compute all the full ρ_i . If N denotes the total number of points, $\tilde{N} = \max N_i$ and $\tilde{N}_s = \max N_{s,i}$, then this step will take $O(n\tilde{N}^3 + n^2\tilde{N}\tilde{N}_s) = O(N\tilde{N}^2 + N^2\tau)$ time. We are thus free to multiply each row of (5.3) by X_i , giving rows of the form

$$\hat{\rho}_i + \sum_{j \neq i} X_i A_{ii}^{-1} E_i \hat{A}_{ij} \hat{\rho}_j = X_i A_{ii}^{-1} h_i. \quad (5.4)$$

If we let $S_{ii} = X_i A_{ii}^{-1} E_i$ and multiply each row by S_{ii}^{-1} , we arrive at the reduced linear system

$$\begin{pmatrix} S_{11}^{-1} & \hat{A}_{12} & \cdots & \hat{A}_{1n} \\ \vdots & & & \vdots \\ \hat{A}_{n1} & \cdots & \hat{A}_{n(n-1)} & S_{nn}^{-1} \end{pmatrix} \begin{pmatrix} \hat{\rho}_1 \\ \vdots \\ \hat{\rho}_n \end{pmatrix} = \begin{pmatrix} S_{11}^{-1} X_1 A_{11}^{-1} h_1 \\ \vdots \\ S_{nn}^{-1} X_n A_{nn}^{-1} h_n \end{pmatrix}. \quad (5.5)$$

Due to the restriction that \hat{A}_{ij} is a sub-matrix of A , this reduced matrix has the same structure as A . The above compression scheme can therefore be repeated with larger boxes \tilde{B}_i until the reduced system is small enough to solve directly. This idea forms the basis of fast algorithms such as the recursive skeletonization algorithm [28]. There also exist more sophisticated approaches such as [41, 54], which relax the requirement that (5.2) holds for all $i \neq j$, which reduces the size of the low rank factorizations, and so achieves an $O(NM)$ scaling algorithm. In our experiments below, we use an extension of the method presented in [54], allowing us to build a fast direct solver for (4.4) in $O(NM)$ time, albeit with a larger constant.

In the above, for ease of exposition we have assumed that the matrices S_{ii} are invertible. This is not required in actual implementations. We stress that in order for an algorithm to beat the naive matrix-vector multiplication cost $O(N^2)$, the compression step (5.2) must be done without computing all of the matrix entries of A . It is here where the particular structure and analytical properties of the kernels must be leveraged. In the following section we discuss a method for efficiently constructing these factorizations.

5.1 Construction of the low rank factorizations

We now discuss how to build the factorizations (5.1) without needing to form the entire matrix A . In this section we describe how to construct the X_j 's. The intuition for the E_i 's is analogous, with a few modifications described in the next section. The method described in this section is based on an extension of the *proxy surface* method [59, 61], which was used to build the fast direct solver in [54]. Our extension is a special case of the work in [59] which applies to general kernels, but the structure of our kernels will allow us to prove that our ranks do not grow as the box sizes do and to give more explicit error bounds.

When constructing the boxes B_i , we can choose centers \mathbf{x}_i and ensure that each box B_i lives in the ball $B_\rho(\mathbf{x}_i)$. When $\|\mathbf{x}_i - \mathbf{x}_j\| > (1+c)\rho$, these blocks are said to be “well-separated”. We will choose ρ large enough so that the matrix entries corresponding to points in well-separated boxes are evaluated using the farfield quadrature. For simplicity we assume that this is obtained by taking the kernels evaluated at source and target points multiplied by a smooth quadrature weight depending only on the source.

We begin by describing a method for efficiently constructing an X_j such that

$$A_{ij} \approx \tilde{A}_{ij} X_j, \quad (5.6)$$

where \tilde{A}_{ij} is a sub-matrix of A_{ij} , for all i such that B_i and B_j are well separated. Throughout this section, we let $\mathbf{r}'_1, \dots, \mathbf{r}'_N$ be the discretization nodes in B_j and \mathbf{r}_1, \dots are the rest of the discretization nodes.

We begin with the following lemma, which is an easy extension of the observation in [55].

Lemma 6. *Let $r = \sqrt{(x_1 - y_1)^2 + (x_2 - y_2)^2}$. Then*

$$-\log r \delta_{ij} + \frac{(x_i - y_i)(x_j - y_j)}{r^2} = -(\delta_{ij} + x_j \partial_{x_i}) \log r + y_j \partial_{x_i} \log r. \quad (5.7)$$

for $1 \leq i, j \leq 2$.

This lemma readily implies that the kernel K_T associated with \mathcal{K}_T is of the general form

$$\begin{aligned} K_T(\mathbf{r}, \mathbf{r}') &= \sum_{0 \leq j_1 + j_2 + j_3 \leq 3} \sum_{0 \leq i_1 + i_2 + i_3 \leq 1} A_{j_1, j_2, j_3}^{i_1, i_2, i_3}(\mathbf{r}) r_1^{i_1} r_2^{i_2} r_3^{i_3} \partial_{r_1}^{j_1} \partial_{r_2}^{j_2} \partial_{r_3}^{j_3} \log \|\mathbf{r} - \mathbf{r}'\| B_1(\mathbf{r}') \\ &+ \sum_{0 \leq j_1 + j_2 + j_3 \leq 3} \sum_{0 \leq i_1 + i_2 + i_3 \leq 1} A_{j_1, j_2, j_3}^{i_1, i_2, i_3}(\mathbf{r}) r_1^{i_1} r_2^{i_2} r_3^{i_3} \partial_{r_1}^{j_1} \partial_{r_2}^{j_2} \partial_{r_3}^{j_3} \log \|\mathbf{r} - \mathbf{r}'\| B_2(\mathbf{r}') \\ &+ \sum_{0 \leq j_1 + j_2 + j_3 \leq 3} \sum_{0 \leq i_1 + i_2 + i_3 \leq 1} A_{j_1, j_2, j_3}^{i_1, i_2, i_3}(\mathbf{r}) r_1^{i_1} r_2^{i_2} r_3^{i_3} \partial_{r_1}^{j_1} \partial_{r_2}^{j_2} \partial_{r_3}^{j_3} \log \|\mathbf{r} - \mathbf{r}'\| B_3(\mathbf{r}'), \end{aligned} \quad (5.8)$$

where the 4×4 coefficient tensors $A_{j_1, j_2, j_3}^{i_1, i_2, i_3}$ depend on $\mathbf{n}(\mathbf{r})$, $S(\mathbf{r})$ and $H(\mathbf{r})$, and the entries of the 4×4 matrix-valued functions $B^j(\mathbf{r}')$ are polynomials in \mathbf{r}' and $\mathbf{n}(\mathbf{r}')$.

In light of (5.8), if ρ_j is the subset of entries of the density corresponding to box B_j , the vector $A_{i,j} \rho_j$, can be written as a combination of functions of the form

$$\varphi(\mathbf{r}) := \sum_{0 \leq j_1 + j_2 + j_3 \leq 3} \sum_{0 \leq i_1 + i_2 + i_3 \leq 1} C_{j_1, j_2, j_3}^{i_1, i_2, i_3} r_1^{i_1} r_2^{i_2} r_3^{i_3} \partial_{r_1}^{j_1} \partial_{r_2}^{j_2} \partial_{r_3}^{j_3} \sum_{k=1}^N \log \|\mathbf{r} - \mathbf{r}'_k\| \tilde{\rho}_k, \quad (5.9)$$

evaluated at the targets in box i , where $\tilde{\rho}_k$ includes factors like ω_k and $B(\mathbf{r}'_k)$, with some terms multiplied by diagonal operators corresponding to surface properties. Each φ can be expressed as a differential operator \mathcal{C} applied to the function

$$\psi(\mathbf{r}) := \sum_{k=1}^N \log \|\mathbf{r} - \mathbf{r}'_k\| \tilde{\rho}_k. \quad (5.10)$$

The following lemma enables the explicit expansion of (5.10) in terms of spherical harmonics. For ease of exposition, we assume that all spherical coordinate systems in this section are centered at \mathbf{x}_j .

Lemma 7. *If $\mathbf{x} = (R, \theta, \varphi)$ in spherical coordinates and $R > r = \|\mathbf{y}\|$, then*

$$\log \|\mathbf{x} - \mathbf{y}\| = \log R - \sum_{n=1}^{\infty} \frac{a_n}{R^n} \sum_{l=0}^n L_{nl} \sqrt{\frac{4\pi}{2l+1}} \sum_{m=-l}^l Q_m^l Y_m^l(\theta, \varphi), \quad (5.11)$$

where $a_n = \frac{r^n}{n}$, L_{nl} is defined below and $Q^l = Q^l(\mathbf{y})$ is a normalized vector of length $2l+1$ for each $l \geq 0$.

Proof. The two-dimensional multipole expansion (see [34]) gives that

$$\log \|\mathbf{x} - \mathbf{y}\| = \log R - \sum_{n=1}^{\infty} \frac{\cos(n\theta_s) r^n}{R^n n}, \quad (5.12)$$

where θ_s is the angle between \mathbf{x} and \mathbf{y} . We now seek to express the right-hand side of the above equation as a function of the polar angles θ and φ . First we write $\cos(n\theta_s)$ as a sum of Legendre polynomials:

$$\cos(n\theta_s) = T_n(\arccos(\theta_s)) = \sum_{l=0}^n L_{nl} P_l(\arccos(\theta_s)), \quad (5.13)$$

where T_n is a Chebyshev polynomial, P_l is a Legendre polynomial, and the coefficients L_{nl} are

$$L_{nl} = \begin{cases} 1 & n = l = 0 \\ \frac{\sqrt{\pi}}{2A(n)} & n = l > 0 \\ \frac{-n(l+1/2)}{(n+l+1)(n-l)} A\left(\frac{n-l-2}{2}\right) A\left(\frac{n+l-1}{2}\right) & n > l \text{ and } n+l \text{ is even} \\ 0 & \text{otherwise} \end{cases}, \quad (5.14)$$

with $A(z) = \frac{\Gamma(z+1/2)}{\Gamma(z+1)}$ (see [1]). Noting that $P_l(\arccos(\theta_s)) = \sqrt{\frac{4\pi}{2l+1}} Y_l^0(\theta_s, 0)$ and using the rotation formula for spherical harmonics, (5.13) becomes

$$\cos(n\theta_s) = \sum_{l=0}^n L_{nl} \sqrt{\frac{4\pi}{2l+1}} Y_l^0(\theta_s, 0) = \sum_{l=0}^n L_{nl} \sqrt{\frac{4\pi}{2l+1}} \sum_{m=-l}^l Q_m^l Y_l^m(\theta, \varphi). \quad (5.15)$$

With this choice of normalization, the spherical harmonics are an orthonormal basis for L^2 on the sphere, and so Q^l is a vector of norm 1. Substituting this expression into (5.12) gives (5.11). \square

In order to truncate the sums, we must control the behavior of L_{nl} for large n . Lemma 2.4 in [1] states that

$$\frac{e^{-1/2}}{\sqrt{z+1}} \leq |A(z)| \leq \frac{e}{\sqrt{|z+1|}} \quad (5.16)$$

for all $z \geq 0$. Using these inequalities, the following lemma establishes a bound for L_{nl} .

Lemma 8. *There is a $C > 0$ such that $|L_{nl}| \leq C\sqrt{n+1}$ for all $0 \leq l \leq n$.*

Proof. If $l \leq n-2$, we can use (5.16) to bound

$$|L_{nl}| \leq \frac{n(l+1/2)}{(n+l+1)(n-l)} \frac{2e^2}{\sqrt{(n-l-2+2)(n+l-1+2)}} \leq \frac{n(n-3/2)e^2}{(n+1)^{3/2}\sqrt{2}} \leq \frac{e^2}{\sqrt{2}} \sqrt{n+1}. \quad (5.17)$$

We can also bound the remaining non-zero terms using (5.16): $L_{nn} \leq \frac{\sqrt{\pi e}}{2} \sqrt{n+1}$. Combining these bounds gives the result. \square

The previous two lemmas immediately imply the following decomposition of ψ .

Corollary 2.3. *Let ψ be as defined in (5.10). Then*

$$\psi(\mathbf{r}) = \sqrt{4\pi} \log(\|\mathbf{r}\|) \alpha_{0,0,0} - \sum_{\ell=0}^{\infty} \sum_{m=-\ell}^{\ell} Y_m^{\ell}(\theta_{\mathbf{r}}, \varphi_{\mathbf{r}}) \sum_{n=\max(\ell,1)}^{\infty} \frac{\rho^n}{n\|\mathbf{r}\|^n} \alpha_{n,\ell,m} \quad (5.18)$$

with

$$\alpha_{n,\ell,m} = \sqrt{\frac{4\pi}{2\ell+1}} L_{n,\ell} \sum_{k=1}^N \frac{\|\mathbf{r}'_k\|^n}{\rho^n} Q_m^{\ell}(\theta_{\mathbf{r}'_k}, \varphi_{\mathbf{r}'_k}) \tilde{\rho}_k.$$

Moreover, there exists a global constant C independent of n, ℓ and m such that the coefficients $\alpha_{n,\ell,m}$ are bounded by

$$|\alpha_{n,\ell,m}| \leq C \sqrt{\frac{n+1}{\ell+1}} \sum_{k=1}^N |\tilde{\rho}_k|.$$

In particular, if the series is truncated at $\ell = L$, the absolute value of the truncation error, \mathcal{E}_L , is bounded by

$$\mathcal{E}_L \leq C'' L^2 \log(\|\mathbf{r}\|/\rho)^{-1} \left(\frac{\rho}{\|\mathbf{r}\|} \right)^L \sum_{k=1}^N |\tilde{\rho}_k|$$

for some absolute constant C'' . If the series is truncated at $\ell, n \leq L$, then the absolute value of the truncation error satisfies the same estimate.

Proof. The expansion (5.18) and the bounds on $\alpha_{n,\ell,n}$ are a direct consequence of the previous lemmas. The truncation bound can be obtained by bounding the remainder in terms of an integral and using standard properties of the incomplete Γ function. \square

When we build X_j , it will generate an interpolant of ψ . In what follows we use the following approximation theory result to bound the interpolation error.

Theorem 3. Consider a function $g : [0, 1] \rightarrow \mathbb{R}$ of the form

$$g(x) = \sum_{n=1}^{\infty} x^n g_n,$$

with $|g_n| \leq Cn^a$ for some constants $a > -1$ and C . Let $\hat{x}_1, \dots, \hat{x}_P$ be Chebyshev nodes of the first kind [56] shifted and scaled to live in $[0, 1/(1+c)]$ for $c > 0$. If, $|g(\hat{x}_i)| < \epsilon$ for all then

$$|g(x)| \leq D(\log(P+1) + 1) \left(\epsilon + \frac{\zeta^{-P}}{\zeta - 1} \right), \quad (5.19)$$

where $\zeta = c + 1 + \sqrt{c^2 + 2c}$ and D is a constant that depends only on a, c , and C .

Proof. To bound g , we seek a polynomial g_P of degree less than P , which approximates g . To bound the approximation error, we first bound g in a disk centered at 0. If $1/(1+c) < r < 1$, then we can bound $|g(z)|$ as follows,

$$\max_{z \in B_r(0)} |g(z)| \leq \tilde{C} \int_0^{\infty} r^n n^a dn \leq \tilde{C} \frac{\Gamma(a+1)}{\log(1/r)^{a+1}} =: M_r.$$

If we let $h(z) := g((z+1)/2(1+c))$ and $\lambda = 2r(1+c) - 1$, then this result implies that h is bounded by M_r on the Bernstein ellipse with $\rho + 1/\rho = 2\lambda$. It follows that $\rho = \lambda + \sqrt{\lambda^2 - 1}$, and that there exists (see Chapter 8 of [56]) a polynomial h_d of degree less than d such that

$$\|h_P - h\|_{L^\infty([-1,1])} \leq 2M_r \frac{\rho^{-P}}{\rho - 1}.$$

If $g_P(z) := h_P(2z(1+c) - 1)$, then this implies that

$$\sup_{z \in [0, 1/(1+c)]} |g_P(z) - g(z)| \leq \tilde{C} \frac{\Gamma(a+1)}{\log(1/r)^{a+1}} \frac{\rho^{-P}}{\rho - 1}.$$

If we let $r = (1/(1+c) + 1)/2 = (2+c)/2(1+c)$, then we can write ρ in the more explicit form

$$\rho = c + 1 + \sqrt{c^2 + 2c}.$$

Finally, the assumption that $|g(\hat{x}_i)| < \epsilon$ implies that $|g_d(\hat{x}_i)| \leq \epsilon + C \frac{\Gamma(p+1)}{\log(1/r)^{p+1}} \frac{\rho^{-d}}{\rho - 1}$. Since g_d is a polynomial, we can bound it on the whole interval $[0, 1/(1+c)]$ by these values time the Lebesgue constant Λ_d . Since the Lebesgue is bounded by $\frac{2}{\pi} \log(d+1) + 1$, this proves the result. \square

Theorem 4. Let $\{\mathbf{p}'_p\}$ be a collection of quadrature nodes on the unit sphere that exactly integrate $Y_m^\ell(\boldsymbol{\theta}) \overline{Y_{m'}^{\ell'}}(\boldsymbol{\theta})$ for $0 \leq \ell, \ell' \leq L$, and $-\ell \leq m \leq \ell, -\ell' \leq m' \leq \ell'$. Let $\hat{x}_1, \dots, \hat{x}_P$ be P Chebyshev nodes of the first kind in the interval $[0, 1/(1+c)\rho]$. Also let

$$v(\mathbf{r}) = \sum_{\ell=0}^{\infty} \sum_{m=-\ell}^{\ell} Y_m^\ell(\boldsymbol{\theta}_{\mathbf{r}}, \varphi_{\mathbf{r}}) \sum_{n=\max(\ell,1)}^{\infty} \frac{\rho^n}{\|\mathbf{r}\|^n} \gamma_{n,\ell,m}, \quad (5.20)$$

where $|\gamma_{n,\ell,m}| < C/\sqrt{n+1}$.

If $\mathbf{p}_{p,p'} = \frac{\mathbf{p}'_p}{\hat{x}_p}$ and $|v(\mathbf{p}_{p,p'})| < \epsilon$ for all p and p' , then

$$|v(\mathbf{r})| \leq DL^2(\log(P+1)+1) \left(\epsilon + \frac{\zeta^{-P}}{\zeta-1} \right) + DL^2 \log(1+c)^{-1} (1+c)^{-L} \quad (5.21)$$

for all $\mathbf{r} \in B_R(\mathbf{x}_j) \setminus B_{(1+c)\rho}(\mathbf{x}_j)$, where D is a constant independent of v and L , and $\zeta < 1$ is the constant given in Theorem 3.

Proof. To bound v , we split it into the $\ell \leq L$ terms, denoted v_1 , and the remainder v_2 . For all $0 \leq |m| \leq \ell \leq L$, we let

$$v_1^{m,\ell}(r) = \int_S v_1^{m,\ell}(r, \boldsymbol{\theta}) \overline{Y_m^\ell(\boldsymbol{\theta})} dA(\boldsymbol{\theta}) = \sum_p v_1^{m,\ell}(r, \boldsymbol{\theta}_p) \overline{Y_m^\ell(\boldsymbol{\theta}_p)} = \sum_{n=\ell}^{\infty} \frac{\rho^n}{nr^n} \gamma_{n,\ell,m}. \quad (5.22)$$

be the spherical Fourier coefficient of v_1 at each r . The choice of nodes $\mathbf{p}_{p,p'}$ and assumption that v_1 is small at these nodes guarantees that

$$|v_1^{m,\ell}(1/\hat{x}_{p'})| \leq \epsilon \sum_p |\tau_p|, \quad (5.23)$$

where τ_p are the quadrature weights associated with the spherical quadrature nodes \mathbf{p}'_p . Applying Theorem 3 with $x = \rho/r$ gives that

$$|v_1^{m,\ell}(r)| \leq C(\log(P+1)+1) \left(\epsilon \sum_p |\tau_p| + \frac{\zeta^{-P}}{\zeta-1} \right) \quad (5.24)$$

for all $r \in [(1+c)\rho, R]$. Since

$$v_1(r, \boldsymbol{\theta}) = \sum_{\ell=0}^N \sum_{m=-\ell}^{\ell} v_1^{m,\ell}(r) Y_\ell^m(\boldsymbol{\theta}), \quad (5.25)$$

this result implies that $|v_1(r, \boldsymbol{\theta})| \leq DL^2(\log(P+1)+1) \left(\epsilon \sum_p |\tau_p| + \frac{\zeta^{-P}}{\zeta-1} \right)$ for all $r \in [(1+c)\rho, R]$.

The remainder v_2 can easily be bounded by Corollary 2.3 and so this proves the result. \square

The result can be easily extended to bound $\mathcal{C}[v]$ using Lemmas 9 and 10 in Appendix A.

Corollary 4.1. *If v satisfies the same assumptions as Theorem 4, then $\mathcal{C}[v]$ satisfies a bound equivalent to (5.21) multiplied by R and L raised to powers that depend on the order of the polynomials and differential operators in \mathcal{C} .*

To construct the matrix X_j , we choose R large enough so that $B_R(\mathbf{x}_j)$ covers Γ , and lay down proxy points $\mathbf{p}_1, \dots, \mathbf{p}_P$ covering $B_R(\mathbf{x}_j) \setminus B_{(1+c)\rho}(\mathbf{x}_j)$. We then construct the matrix D with entries

$$D_{p,k} = \log \|\mathbf{p}_p - \mathbf{r}'_k\| - \log \|\mathbf{p}_p - \mathbf{x}_j\| \quad (5.26)$$

for all k such that $\mathbf{r}'_k \in B_j$. We also append a row of ones to D . Corollary 2.3 implies that $D_{p,k}$ admits an approximate low rank factorization with a rank that scales as $(\log \epsilon / \log(1+c))^3$. In particular, for any $\epsilon > 0$, we can construct its interpolative decomposition [9], which finds a matrix \tilde{D} composed of columns k_1, \dots, k_{N_s} of D and a matrix \tilde{X}_j such that

$$\|D - \tilde{D}\tilde{X}_j\|_\infty \leq \epsilon. \quad (5.27)$$

Further, the factorization can be chosen so that columns k_1, \dots, k_{N_s} of \tilde{X}_j form the identity matrix. To see the advantage of this property, we let $\hat{\rho}_s = \sum_k (X_j)_{s,k} \tilde{\rho}_k$ and define the function

$$\tilde{\psi}(\mathbf{r}) := \sum_{s=1}^{N_s} \log \|\mathbf{r} - \mathbf{r}'_{k_s}\| \hat{\rho}_s = \sum_{s=1}^{N_s} (\log \|\mathbf{r} - \mathbf{r}'_{k_s}\| - \log \|\mathbf{r} - \mathbf{x}_j\|) \hat{\rho}_s + \log \|\mathbf{r} - \mathbf{x}_j\| \sum_{s=1}^{N_s} \hat{\rho}_s. \quad (5.28)$$

By construction $\sum_s \hat{\rho}_s = \sum_k \tilde{\rho}_k$, and so $\tilde{\psi}(\mathbf{p}_p) = (\tilde{D}\tilde{X}_j\rho)_k + \log \|\mathbf{p}_p - \mathbf{x}_j\| \sum_k \tilde{\rho}_k$. The definition (5.27) thus gives that $|\psi(\mathbf{p}_p) - \tilde{\psi}(\mathbf{p}_p)| < \epsilon \max |\tilde{\rho}_k|$ for all p . We now argue that, provided proxy nodes are well-chosen, this is sufficient to guarantee that $\varphi \approx \mathcal{C}[\tilde{\psi}]$ and so \tilde{X}_j can be used to construct the desired X_j .

The function $v = \psi - \tilde{\psi}$ satisfies the assumptions of Theorem 4. Since K_T is a combination of functions of the form of $\mathcal{C}[\psi]$, for various \mathcal{C} (multiplied by properties such as the mean curvature), Theorem 4 directly implies the following corollary, which is the main result of this section.

Corollary 4.2. *Let \tilde{X}_j be the low rank factorization defined in (5.27). If $X_j = \tilde{X}_j \otimes I_4$, then $A_{ij} \approx \tilde{A}_{ij}X_j$ for all i such that B_i is well-separated from B_j . Further, the approximation error is $O(L^5 \log L(\epsilon + \zeta^{-L}))$.*

The 5th power in the error bound is due to the formulas in Lemma 10 and the fact that the differential operators \mathcal{C} are at most third order.

Our method for computing X_j can be summarized in the following algorithm

Algorithm 1 Computation of the matrix X_j

1. Lay down proxy points \mathbf{p}_p lying in a sequence of spheres centered at \mathbf{x}_j with radii covering $[(1+c)\rho, \infty)$, as described in Theorem 4.
 2. Evaluate the matrix D with entries $D_{p,k} = \log \|\mathbf{p}_p - \mathbf{r}'_k\| - \log \|\mathbf{p}_p - \mathbf{x}_j\|$ for every \mathbf{r}'_k in B_j and every proxy point \mathbf{p}_p .
 3. Append a row of ones to D .
 4. Evaluate $K_T(\mathbf{r}_k, \mathbf{r}_{k'})$ for every pair of points with $\mathbf{r}_k \in B_{(1+c)\rho}(\mathbf{x}_j) \setminus B_j$ and $\mathbf{r}_{k'} \in B_j$ and append these rows to D .
 5. Compute the interpolative decomposition $D = \tilde{D}\tilde{X}_j$ where columns k_1, \dots, k_{N_s} of \tilde{X}_j form an identity block.
 6. Define $X_j = \tilde{X}_j \otimes I_4$.
-

Step 4 in this algorithm ensures that the matrix X_j can also be used for compressing the interaction of B_j with B_i , even when they are not well-separated. In some compression schemes, such as [41, 54], this step should be omitted.

The construction of the E_i matrices is analogous to the procedure for constructing X_j 's, except that this time the differential operator \mathcal{C} involves derivatives with respect to the target positions \mathbf{r}_k in the ball $B_\rho(\mathbf{x}_i)$. We must therefore build the interpolative decomposition of a matrix containing all of our kernels, rather than just the archetypal logarithm. This procedure is summarized in the following algorithm.

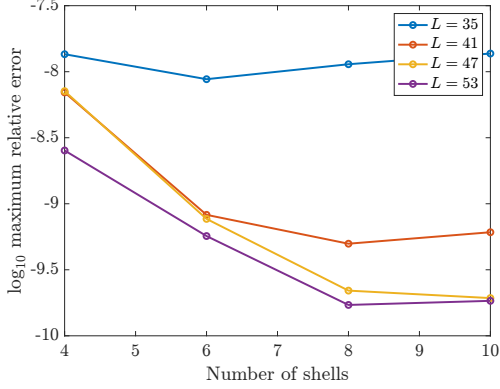


Figure 3: The maximum error in the compressed approximation of the logarithmic kernel found in the test described in Section 6.1. It is plotted as a function of the number of proxy shells and the order of the quadrature scheme on each shell.

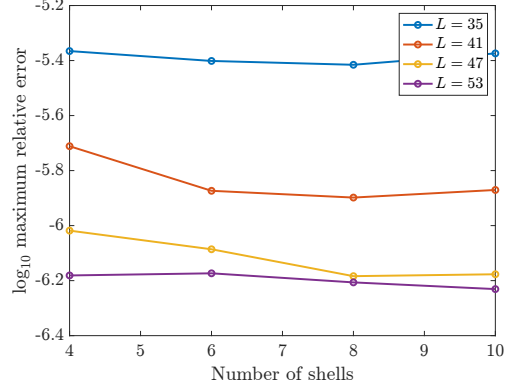


Figure 4: The maximum error in the compressed approximation of the remainder kernel found in the test described in Section 6.1. It is plotted as a function of the number of proxy shells and the order of the quadrature scheme on each shell.

Algorithm 2 Computation of the matrix E_i

1. Lay down proxy points \mathbf{p}_p lying in a sequence of spheres centered at \mathbf{x}_i with radii covering $[(1+c)\rho, \infty)$, as described in Theorem 4.
 2. Evaluate the block matrix D with entries $D_{k,p} = K_T(\mathbf{r}_k, \mathbf{p}_p)$ for every \mathbf{r}_k in B_i and every proxy point \mathbf{p}_p , where the different components of K_T are organized into different rows.
 3. Evaluate $K_T(\mathbf{r}_k, \mathbf{r}_{k'})$ for every pair of points with $\mathbf{r}_k \in B_{(1+c)\rho}(\mathbf{x}_i) \setminus B_i$ and $\mathbf{r}_{k'} \in B_j$ and append these rows to D .
 4. Compute the interpolative decomposition $D = \tilde{E}_i \hat{D}$ where rows k_1, \dots, k_{N_s} of \tilde{E}_i form an identity block.
 5. Define $E_i = \tilde{E}_i \otimes I_4$.
-

As for X_j , the interaction with points in neighboring boxes should be omitted in some compression schemes.

6 Numerical Illustrations

In this section we illustrate the effectiveness of our compression scheme and test our solver on a few different surfaces.

6.1 Compression

We begin by testing the compression scheme described in Section 5.1 with $\rho = 1$, $R = 1000$, and $c = 1$. We distribute 5 000 points uniformly in $B_1(0)$ and 5 000 points uniformly in $B_{1000}(0) \setminus B_2(0)$. For the purposes of this test, we set the surface parameters that appear in K_T to be random numbers uniformly distributed in $[-1, 1]$.

We lay down proxy shells in the method summarized in Theorem 4. On each shell, we use L th order Lebedev nodes. We build the matrix D given by (5.26) and build an interpolative decomposition with tolerance 10^{-10} . The resulting maximum errors in the approximations of the logarithm of the distance between points is shown in Figure 3. The resulting maximum errors in the approximation of K_T are shown in Figure 4.

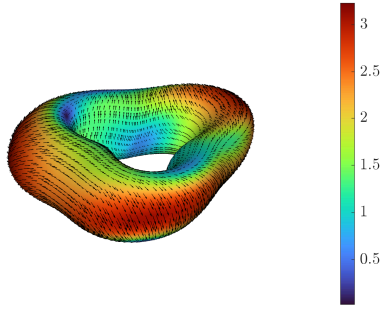


Figure 5: The reference solution \mathbf{u} used for the convergence test with errors in Figure 7. The color indicates the norm of \mathbf{u} .

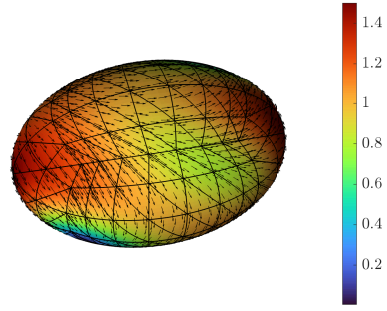


Figure 6: The reference solution \mathbf{u} used for the ellipsoid test. The black lines show the mesh and the color indicates the norm of \mathbf{u} .

6.2 Convergence test

Having demonstrated the effectiveness of our compression scheme, we now test the convergence of our solver. In this example, we choose the surface Γ to be the surface parameterized by

$$\mathbf{r}(u, v) = \begin{pmatrix} 1 & 0 & 1/2 \\ 0 & 1 & 0 \\ 0 & 0 & 1 \end{pmatrix} \left[\begin{pmatrix} \left(2 + \frac{3}{4} \cos(v) + \frac{3}{4} \cos(3u)\right) \cos(u) \\ \left(2 + \frac{3}{4} \cos(v) + \frac{3}{4} \cos(3u)\right) \sin(u) \\ \frac{3}{4} \sin(v) \end{pmatrix} - \begin{pmatrix} 1.5 \\ 0 \\ 0 \end{pmatrix} \right] + \begin{pmatrix} 1.5 \\ 0 \\ 0 \end{pmatrix}. \quad (6.1)$$

To test the solver, we choose the right hand side so that the true solution is $u = P(z, x, y)^T$ and $p = z$. This true solution is shown in Figure 5. We construct the right hand side using the 24th order spectral differentiation implements in the surfacefun package [15]. We then discretize the surface using an increasing number of 8th order tensor product Gauss-Legendre quadrilateral patches and construct a fast direct solver for (3.23) and fast apply for evaluating the representation and recovering the velocity \mathbf{u} with compression and quadrature tolerances set to 10^{-7} . The resulting relative Frobenius errors in the velocity (Figure 7) show that the error in our solver is comparable to the requested tolerance. In Figure 8 we show the time to construct the fast direct solver for (3.23), which is the dominant cost in our solver. We can see that the cost scales linearly as we refine our surface discretization. In all of these experiments, the number of degrees of freedom is three times the number of discretization nodes, n_{pts} .

As another example, we solve the surface Stokes equations on an ellipsoid with axis lengths 1.5, 1, and 1. To remove the null space discussed in remark 3, we add the term \mathbf{u} to the first equation

$$-\frac{1}{2} \mathcal{P} \nabla_{\Gamma} \cdot (\nabla_{\Gamma} \mathbf{u} + (\nabla_{\Gamma} \mathbf{u})^T) + \mathbf{u} + \nabla_{\Gamma} p = \mathbf{f}$$

and modify (3.23) accordingly. For this test, we discretize the ellipsoid with 288 eighth-order triangular patches (12 960 points), set our integration tolerance to 10^{-9} and compression tolerance to 10^{-8} . The relative Frobenius error in the manufactured solution test (Figure 6) with $\mathbf{u} = P(z, x, y)^T$ and $p = z$ was 3.2982×10^{-8} .

As a final example, we consider the surface Stokes equation on the surface is parameterized by

$$\mathbf{r}(u, v) = \begin{pmatrix} 1 & 0 & 1/2 \\ 0 & 1 & 0 \\ 0 & 0 & 1 \end{pmatrix} \left[\begin{pmatrix} \left(\frac{3}{5} + \left(\frac{1}{2} + \frac{1}{10} \cos(5v)\right) \cos(v)\right) \cos(u) \\ \left(\frac{3}{5} + \left(\frac{1}{2} + \frac{1}{10} \cos(5v)\right) \cos(v)\right) \sin(u) \\ \left(\frac{1}{2} + \frac{1}{10} \cos(5v)\right) \sin(v) \end{pmatrix} - \begin{pmatrix} 1.5 \\ 0 \\ 0 \end{pmatrix} \right] + \begin{pmatrix} 1.5 \\ 0 \\ 0 \end{pmatrix}. \quad (6.2)$$

We discretize this surface using 16 384 points arranged in 256 eighth-order quadrilateral patches (Figure 9). We choose the right hand side $\mathbf{f} = 0$ and choose g to be a difference of functions of the form $e^{-3(\mathbf{x} - \mathbf{x}_0)^2}$ centered at $\mathbf{x}_0 = (-1.6, 1, 0.2)^T$ and $\mathbf{x}_0 = (1.5, 0, 0.4)^T$. We make the coefficient of the second term negative and scale the two Gaussians so that g satisfies the mean zero consistency condition. The resulting solution is shown in Figure 10.

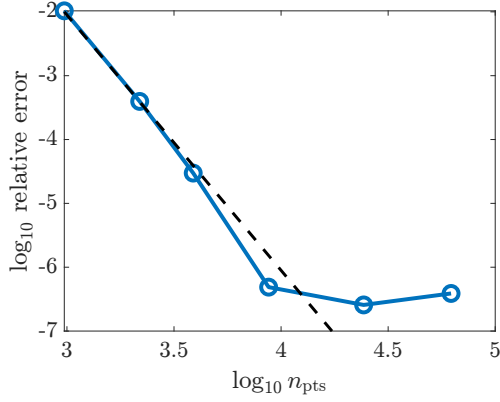


Figure 7: The relative error L^2 error in \mathbf{u} for an analytical solution test on a slanted torus. The black dashed line indicates 8th order convergence. The true solution is shown in Figure 5.

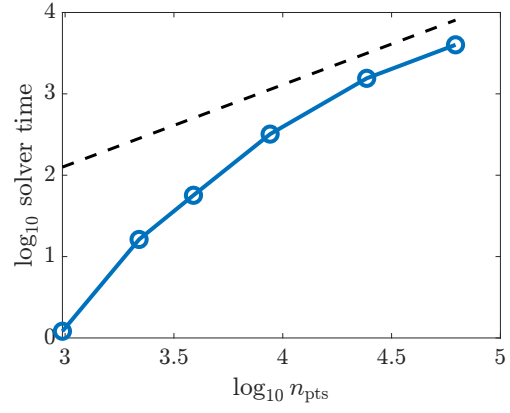


Figure 8: The times to build the inverse for (3.23) versus the number of surface discretization nodes. The tests were run on an Apple MacBook Pro with an M2 Max chip. The black dashed line indicates $O(n_{\text{pts}})$ time.

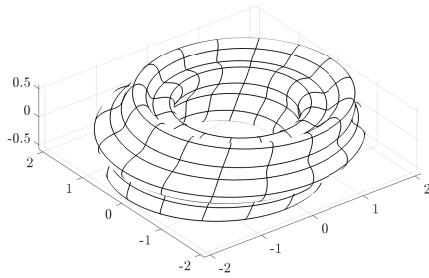


Figure 9: The mesh used to discretize the surface in Figure 10.

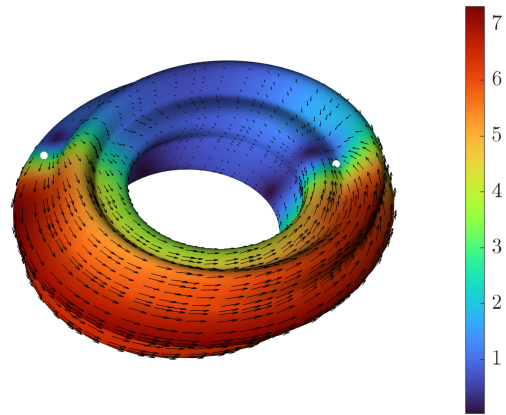


Figure 10: An example solution generated by a fluid source and sink centered at the white dots.

7 Conclusion

In this paper we have described a numerical approach for solving the surface Stokes equations on arbitrary smooth manifolds embedded in three dimensions. The method is based on introducing suitable parametrices that convert the surface PDEs associated with the Stokes equations into a coupled system of integral equations for an unknown vector-valued surface density. We have shown that this resulting system is a Fredholm integral equation of the second kind, which upon discretization typically leads to linear systems which are well-conditioned under mesh refinement. However, the resulting discrete systems are dense, with non-zero entries between degrees of freedom corresponding to even well-separated points. To overcome this difficulty, we adapted a standard fast algorithm for forming compressed representations of the inverse of these linear systems. This broad class of methods is based on the observation that the rank of interaction between physically well-separated sets of points is low. For our particular kernels, we prove this fact and provide the bounds for the interaction ranks. These estimates are potentially interesting in their own right, and the proof techniques apply to a much broader class of problems. In fact the fast direct solver demonstrated here can be used to efficiently solve time dependent surface Stokes problems, nonlinear parabolic equations (see [15]). The presented method can also be extended to solve other surface PDEs, such as the matrix-valued time-harmonic elastodynamic equation or fourth order thin-plate problems.

8 Acknowledgements

J.G.H. was supported in part by a Sloan Research Fellowship. This research was supported in part by grants from the NSF (DMS-2235451) and Simons Foundation (MPS-NITMB-00005320) to the NSF-Simons National Institute for Theory and Mathematics in Biology (NITMB). Contributions by staff of NIST, an agency of the U.S. Government, are not subject to copyright protection within the United States. Certain commercial software used in this paper is identified for informational purposes only, and does not imply recommendation of or endorsement by the National Institute of Standards and Technology, nor does it imply that the products so identified are necessarily the best available for the purpose.

A Spherical harmonic identities

In the interest of making the proofs as self-contained as possible, in this section we briefly summarize several standard properties of spherical harmonics used in the construction of certain low rank factorizations. Partly to fix notation, we start with their definition.

Definition 6. Let $\ell \geq 0$ and $-\ell \leq m \leq \ell$. The spherical harmonic Y_m^ℓ is defined by

$$Y_\ell^m(\theta, \varphi) = \sqrt{\frac{2\ell + 1}{4\pi} \frac{(\ell - |m|)!}{(\ell + |m|)!}} P_\ell^{|m|}(\cos \theta) e^{im\varphi}, \quad (\text{A.1})$$

where $\theta \in [0, \pi]$ and $\varphi \in [0, 2\pi)$. Here P_n^m denotes the associated Legendre function

$$P_n^m(x) = (-1)^m (1 - x^2)^{m/2} \frac{d^m}{dx^m} P_n(x),$$

with P_n the n -th order Legendre polynomial.

The following lemma gives a formula for expressing products of x, y, z and spherical harmonics as linear combinations of spherical harmonics. Its proof follows immediately from the definition of the spherical harmonics and standard properties of associated Legendre polynomials, and is omitted.

Lemma 9. Let $\ell \geq 0$ and $-\ell \leq m \leq n$. If (φ, θ, ρ) are the spherical coordinates corresponding to the point (x, y, z) in Cartesian coordinates, then

$$(x \pm iy)Y_\ell^m(\theta, \varphi) = -\rho\sqrt{\frac{(\ell \pm m + \frac{1}{2})^2 - \frac{1}{4}}{4(\ell+1)^2 - 1}}Y_{\ell+1}^{m\pm 1}(\theta, \varphi) + \rho\sqrt{\frac{(\ell \mp m - \frac{1}{2})^2 - \frac{1}{4}}{4\ell^2 - 1}}Y_{\ell-1}^{m\pm 1}(\theta, \varphi) \quad (\text{A.2})$$

$$zY_\ell^m(\theta, \varphi) = \rho\sqrt{\frac{(\ell+1)^2 - m^2}{4(\ell+1)^2 - 1}}Y_{\ell+1}^m(\theta, \varphi) + \rho\sqrt{\frac{\ell^2 - m^2}{4\ell^2 - 1}}Y_{\ell-1}^m(\theta, \varphi) \quad (\text{A.3})$$

with the convention that terms involving $Y_{\ell'}^{m'}$ with $\ell' < |m'|$ are omitted.

Similarly, the derivatives of the spherical harmonics with respect to the Cartesian coordinates can also be expressed again as linear combinations of spherical harmonics. We summarize these identities in the following lemma.

Lemma 10. Let $\ell \geq 0$ and $-\ell \leq m \leq n$. If (φ, θ, ρ) are the spherical coordinates corresponding to the point (x, y, z) in Cartesian coordinates, then

$$\partial_\pm Y_\ell^m(\theta, \varphi) = \pm \frac{\ell+1}{\rho} \sqrt{\frac{(\ell \mp m - \frac{1}{2})^2 - \frac{1}{4}}{4\ell^2 - 1}} Y_{\ell-1}^{m+1}(\theta, \varphi) \pm \frac{\ell}{\rho} \sqrt{\frac{(\ell \mp m + \frac{3}{2})^2 - \frac{1}{4}}{4(\ell+1)^2 - 1}} Y_{\ell+1}^{m+1}(\theta, \varphi) \quad (\text{A.4})$$

$$\partial_z Y_\ell^m(\theta, \varphi) = \frac{\ell+1}{\rho} \sqrt{\frac{\ell^2 - m^2}{4\ell^2 - 1}} Y_{\ell-1}^m(\theta, \varphi) - \frac{\ell}{\rho} \sqrt{\frac{(\ell+1)^2 - m^2}{4(\ell+1)^2 - 1}} Y_{\ell+1}^m(\theta, \varphi) \quad (\text{A.5})$$

with $\partial_\pm = \partial_x \pm i\partial_y$.

Proof. The proof follows straightforwardly, if tediously, from identity (3.31) in [18], which with our sign conventions becomes

$$\partial_\pm^m \partial_z^{\ell-m} \frac{1}{\rho} = (-1)^{\ell+m} (\ell-m)! \frac{1}{\rho^{\ell+1}} P_\ell^m(\cos \theta) e^{\pm im\varphi}, \quad \ell \geq m \geq 0, \quad (\text{A.6})$$

combined with the definition of the spherical harmonics (A.1), and Lemma 9. □

References

- [1] B. K. Alpert and V. Rokhlin. A fast algorithm for the evaluation of Legendre expansions. *SIAM Journal on Scientific and Statistical Computing*, 12(1):158–179, 1991.
- [2] M. Arroyo and A. DeSimone. Relaxation dynamics of fluid membranes. *Physical Review E—Statistical, Nonlinear, and Soft Matter Physics*, 79(3):031915, 2009.
- [3] T. Askham, L. G. J. Hoskins, L. Lu, M. O. M. Rachh, F. Vico, and V. Rokhlin. fmm3dbie: FMM-accelerated boundary integral equation solvers.
- [4] T. G. Ayele and M. A. Dagnaw. Boundary-domain integral equation systems to the Dirichlet and Neumann problems for compressible Stokes equations with variable viscosity in 2D. *Mathematical Methods in the Applied Sciences*, 44(12):9876–9898, 2021.
- [5] P. Brandner, T. Jankuhn, S. Praetorius, A. Reusken, and A. Voigt. Finite element discretization methods for velocity-pressure and stream function formulations of surface Stokes equations. *SIAM Journal on Scientific Computing*, 44(4):A1807–A1832, 2022.
- [6] P. Brandner and A. Reusken. Finite element error analysis of surface Stokes equations in stream function formulation. *ESAIM: Mathematical Modelling and Numerical Analysis*, 54(6):2069–2097, 2020.

- [7] J. Bremer and Z. Gimbutas. On the numerical evaluation of the singular integrals of scattering theory. *Journal of Computational Physics*, 251:327–343, 2013.
- [8] H. Brenner. *Interfacial transport processes and rheology*. Elsevier, 2013.
- [9] H. Cheng, Z. Gimbutas, P.-G. Martinsson, and V. Rokhlin. On the compression of low rank matrices. *SIAM Journal on Scientific Computing*, 26(4):1389–1404, 2005.
- [10] D. L. Colton, R. Kress, and R. Kress. *Inverse acoustic and electromagnetic scattering theory*, volume 93. Springer, 1998.
- [11] E. Corona, P.-G. Martinsson, and D. Zorin. An $O(N)$ direct solver for integral equations on the plane. *Applied and Computational Harmonic Analysis*, 38(2):284–317, 2015.
- [12] A. Demlow and M. Neilan. A tangential and penalty-free finite element method for the surface Stokes problem. *SIAM Journal on Numerical Analysis*, 62(1):248–272, 2024.
- [13] A. Demlow and M. Neilan. A Taylor-Hood finite element method for the surface stokes problem without penalization. *arXiv preprint arXiv:2506.20419*, 2025.
- [14] W. Fong and E. Darve. The black-box fast multipole method. *Journal of Computational Physics*, 228(23):8712–8725, 2009.
- [15] D. Fortunato. A high-order fast direct solver for surface pdes. *SIAM Journal on Scientific Computing*, 46(4):A2582–A2606, 2024.
- [16] T.-P. Fries. Higher-order surface FEM for incompressible navier-stokes flows on manifolds. *International journal for numerical methods in fluids*, 88(2):55–78, 2018.
- [17] T. Goodwill and M. O’Neil. A parametrix method for elliptic surface PDEs. *Pure and Applied Analysis*, 7(1):171–217, 2025.
- [18] L. Greengard. *The rapid evaluation of potential fields in particle systems*. MIT press, 1988.
- [19] L. Greengard, D. Gueyffier, P.-G. Martinsson, and V. Rokhlin. Fast direct solvers for integral equations in complex three-dimensional domains. *Acta Numerica*, 18:243–275, 2009.
- [20] L. Greengard, M. O’Neil, M. Rachh, and F. Vico. Fast multipole methods for the evaluation of layer potentials with locally-corrected quadratures. *Journal of Computational Physics: X*, 10:100092, 2021.
- [21] L. Greengard and V. Rokhlin. A fast algorithm for particle simulations. *Journal of computational physics*, 73(2):325–348, 1987.
- [22] B. J. Gross and P. J. Atzberger. Hydrodynamic flows on curved surfaces: Spectral numerical methods for radial manifold shapes. *Journal of Computational Physics*, 371:663–689, 2018.
- [23] S. Gross, T. Jankuhn, M. A. Olshanskii, and A. Reusken. A trace finite element method for vector-laplacians on surfaces. *SIAM journal on numerical analysis*, 56(4):2406–2429, 2018.
- [24] N. A. Gumerov and R. Duraiswami. Fast multipole method for the biharmonic equation in three dimensions. *Journal of Computational Physics*, 215(1):363–383, 2006.
- [25] W. Hackbusch and Z. P. Nowak. On the fast matrix multiplication in the boundary element method by panel clustering. *Numerische Mathematik*, 54(4):463–491, 1989.
- [26] H. Hardering and S. Praetorius. Tangential errors of tensor surface finite elements. *IMA Journal of Numerical Analysis*, 43(3):1543–1585, 2023.
- [27] H. Hardering and S. Praetorius. Parametric finite-element discretization of the surface Stokes equations: inf-sup stability and discretization error analysis. *IMA Journal of Numerical Analysis*, 45(5):2948–2987, 2025.

- [28] K. L. Ho. FLAM: Fast linear algebra in MATLAB-algorithms for hierarchical matrices. *Journal of Open Source Software*, 5(51):1906, 2020.
- [29] K. L. Ho and L. Greengard. A fast direct solver for structured linear systems by recursive skeletonization. *SIAM Journal on Scientific Computing*, 34(5):A2507–A2532, 2012.
- [30] K. L. Ho and L. Ying. Hierarchical interpolative factorization for elliptic operators: differential equations. *Communications on Pure and Applied Mathematics*, 69(8):1415–1451, 2016.
- [31] G. C. Hsiao and W. L. Wendland. Boundary integral equations. In *Boundary Integral Equations*, pages 25–94. Springer, 2021.
- [32] L.-M. Imbert-Gerard, F. Vico, L. Greengard, and M. Ferrando. Integral equation methods for electrostatics, acoustics, and electromagnetics in smoothly varying, anisotropic media. *SIAM Journal on Numerical Analysis*, 57(3):1020–1035, 2019.
- [33] T. Jankuhn, M. A. Olshanskii, and A. Reusken. Incompressible fluid problems on embedded surfaces: modeling and variational formulations. *Interfaces and Free Boundaries*, 20(3):353–377, 2018.
- [34] C. Joslin and C. Gray. Multipole expansions in two dimensions. *Molecular Physics*, 50(2):329–345, 1983.
- [35] O. Kilicer. *Higher Order FEM for Surface Stokes Problems*. PhD thesis, 2025.
- [36] K. L. Ho and L. Ying. Hierarchical interpolative factorization for elliptic operators: Integral equations. *Communications on Pure and Applied Mathematics*, 69(7):1314–1353, 2016.
- [37] D. Malhotra, A. Gholami, and G. Biros. A volume integral equation Stokes solver for problems with variable coefficients. In *SC’14: Proceedings of the International Conference for High Performance Computing, Networking, Storage and Analysis*, pages 92–102. IEEE, 2014.
- [38] P.-G. Martinsson. *Fast direct solvers for elliptic PDEs*. SIAM, 2019.
- [39] P.-G. Martinsson and M. O’Neil. Fast direct solvers. *arXiv preprint arXiv:2511.07773*, 2025.
- [40] P.-G. Martinsson and V. Rokhlin. A fast direct solver for boundary integral equations in two dimensions. *Journal of Computational Physics*, 205(1):1–23, 2005.
- [41] V. Minden, K. L. Ho, A. Damle, and L. Ying. A recursive skeletonization factorization based on strong admissibility. *Multiscale Modeling & Simulation*, 15(2):768–796, 2017.
- [42] M. Neilan and H. Wan. A C^0 interior penalty method for the stream function formulation of the surface stokes problem. *ESAIM: Mathematical Modelling and Numerical Analysis*, 59(2):1177–1211, 2025.
- [43] I. Nitschke, A. Voigt, and J. Wensch. A finite element approach to incompressible two-phase flow on manifolds. *Journal of Fluid Mechanics*, 708:418–438, 2012.
- [44] M. A. Olshanskii, A. Quaini, A. Reusken, and V. Yushutin. A finite element method for the surface Stokes problem. *SIAM Journal on Scientific Computing*, 40(4):A2492–A2518, 2018.
- [45] M. A. Olshanskii and V. Yushutin. A penalty finite element method for a fluid system posed on embedded surface. *Journal of Mathematical Fluid Mechanics*, 21(1):14, 2019.
- [46] J. Punchin. Weakly singular integral operators as mappings between function spaces. *The Journal of Integral Equations and Applications*, pages 303–320, 1988.
- [47] M. Rachh. *Integral equation methods for problems in electrostatics, elastostatics and viscous flow*. PhD thesis, New York University, 2015.

- [48] M. Rahimi, A. DeSimone, and M. Arroyo. Curved fluid membranes behave laterally as effective viscoelastic media. *Soft Matter*, 9(46):11033–11045, 2013.
- [49] P. Rangamani, A. Agrawal, K. K. Mandadapu, G. Oster, and D. J. Steigmann. Interaction between surface shape and intra-surface viscous flow on lipid membranes. *Biomechanics and modeling in mechanobiology*, 12(4):833–845, 2013.
- [50] A. Reusken. Stream function Formulation of Surface Stokes Equations.
- [51] S. Reuther and A. Voigt. Solving the incompressible surface Navier-Stokes equation by surface finite elements. *Physics of Fluids*, 30(1), 2018.
- [52] L. E. Scriven. Dynamics of a fluid interface equation of motion for Newtonian surface fluids. *Chemical Engineering Science*, 12(2):98–108, 1960.
- [53] J. C. Slattery, L. Sagis, and E.-S. Oh. *Interfacial transport phenomena*. Springer, 2007.
- [54] D. Sushnikova, L. Greengard, M. O’Neil, and M. Rachh. FMM-LU: A fast direct solver for multiscale boundary integral equations in three dimensions. *Multiscale Modeling & Simulation*, 21(4):1570–1601, 2023.
- [55] A.-K. Tornberg and L. Greengard. A fast multipole method for the three-dimensional Stokes equations. *Journal of Computational Physics*, 227(3):1613–1619, 2008.
- [56] L. N. Trefethen. *Approximation Theory and Approximation Practice, Extended Edition*. SIAM, 2019.
- [57] B. Vioreanu and V. Rokhlin. Spectra of multiplication operators as a numerical tool. *SIAM Journal on Scientific Computing*, 36(1):A267–A288, 2014.
- [58] H. Xiao and Z. Gimbutas. A numerical algorithm for the construction of efficient quadrature rules in two and higher dimensions. *Computers & mathematics with applications*, 59:663–676, 2010.
- [59] X. Xing and E. Chow. Interpolative decomposition via proxy points for kernel matrices. *SIAM Journal on Matrix Analysis and Applications*, 41(1):221–243, 2020.
- [60] J. Yang, Y. Li, and J. Kim. A practical finite difference scheme for the Navier–Stokes equation on curved surfaces in R3. *Journal of Computational Physics*, 411:109403, 2020.
- [61] X. Ye, J. Xia, and L. Ying. Analytical low-rank compression via proxy point selection. *SIAM Journal on Matrix Analysis and Applications*, 41(3):1059–1085, 2020.